NASA Contractor Report 4123

Large-Angle Slewing Maneuvers for Flexible Spacecraft

Hon M. Chun and James D. Turner

Cambridge Research
A Division of Photon Research Associates, Inc.
Cambridge, Massachusetts

NASA

National Aeronautics
and Space Administration

Scientific and Technical
Information Division

1988

ACKNOWLEDGMENT

TABLE OF CONTENTS

TABLE OF CONTENTS (Continued)

SECTION 1

INTRODUCTION

This report summarizes the results of the work performed under NASA contract NAS1-18098 from September 1985 through August 1986. The report is divided into five sections. Section 2 presents a new class of closed-form solutions for finite-time linear-quadratic optimal control problems, which is shown to be computationally more efficient than previously known closed-form solutions. Section 3 utilizes the closed-form solutions of Section 2 for the feedback gains in the free-final-time perturbation feedback problem, where the initial conditions and terminal constraints may be assigned off-nominal values. Section 4 presents a control scheme for general nonlinear three-axis slewing maneuvers of flexible spacecraft. Under this control scheme, an open-loop rigid body nominal solution is applied to the spacecraft while a perturbation feedback controller reduces the elastic response and causes the system to closely follow the nominal rigid body trajectory. A modified Kalman filter is implemented for estimating the states of the system. Section 5 presents a summary and conclusions for this report. Reference 9 documents the detailed derivations of results presented in this report.

SECTION 2

CLOSED-FORM SOLUTIONS FOR FINITE-TIME LINEAR-QUADRATIC
OPTIMAL CONTROL PROBLEMS

2.1   Introduction

During the design and analysis phases of optimal control synthesis,
state and control trajectories are often computed to help the control
engineer evaluate the control design. The most straightforward and most
widely practiced method of computing the state and control trajectories is
by numerically integrating the governing differential equations. This may
be costly for flexible space structures which may have many elastic degrees
of freedom. The reason for the high cost is two-fold: first, the large
number of elastic degrees of freedom requires a large number of states to
be integrated; and second, since the highest frequency of the system to be
simulated increases as the number of elastic modes is increased, the
integration step-size must be decreased correspondingly. Thus, the
computational cost of the simulation increases rapidly as more elastic
degrees of freedom are included.

This section presents a new class of closed-form solutions for
finite-time linear-quadratic optimal control problems when the plant is
time-invariant. With a closed-form solution, one can compute the response
of the entire system at any point in time. Thus, the engineer can compute
the system response at any desired interval, independent of system
frequency. (Of course, if one needs time-history plots with good
resolution, the time interval does depend on system frequency.) In
addition, numerical roundoff errors are greatly reduced, because the number
of floating point operations[1] (flops) required for computing closed-form

----

[1] A floating point operation is more or less the amount of work needed to do
a floating point add, a floating point multiply, and a little subscripting.

solutions is much less than for numerical integration. Sensitivity partials may also be computed easily when closed-form solutions are available [35].

Other forms of closed-form solutions exist. For example, classical state and co-state solutions can be obtained from matrix exponential solutions where the system Hamiltonian matrix is used. However, such solutions either suffer from numerical instability or require too much computation. With a numerically stable and efficient closed-form solution and with the rapid development of parallel processing technology, one may envision the day when feedback gains may be computed on-orbit in real time. Whether the solutions proposed in this chapter can fulfill such a goal is of great interest, and is a subject for further research.

Although there are many different finite-time optimal control problems, their solutions can be written as differential equations of only a few basic forms. The closed-form solutions of these basic differential equations are presented in Section 2.2, and example applications are provided in Section 2.3 for illustration.

2.2 Closed-Form Solutions of Basic Differential Equations

The solution of finite-time linear-quadratic optimal control problems involves the solution of differential equations which may be classified into five basic types:

Type 1

$$\dot{P}(t) = - P(t)A - A^T P(t) + P(t)EP(t) - Q , \qquad (2.2.1)$$

Type 2

$$\dot{X}_1(t) = - [A - EP(t)]^T X_1(t) + F_1(t) , \qquad (2.2.2)$$

Type 3

$$\dot{X}_2(t) = [A - EP(t)]X_2(t) + F_2(t) , \tag{2.2.3}$$

Type 4

$$\dot{Y}_1(t) = X_{1a}^T(t)EX_{1b}(t) , \text{ and} \tag{2.2.4}$$

Type 5

$$\dot{Y}_2(t) = X_{2a}^T(t)Z^{-1}(t)EZ^{-1}(t)X_{2b}(t) . \tag{2.2.5}$$

Type 1 represents the well-known differential matrix Riccati equation with constant coefficients. Its solution, $P(t)$, couples into the differential equations of Type 2 and Type 3. The functions $X_{1a}(t)$ and $X_{1b}(t)$ are solutions of differential equations of Type 2, and the functions $X_{2a}(t)$ and $X_{2b}(t)$ are solutions of differential equations of Type 3. In the above equations, A, E, and Q are $(n \times n)$ constant matrices, and the variables have the following dimensions:

$P(t)$	$(n \times n)$
$X_1(t)$	$(n \times p)$
$X_2(t)$	$(n \times q)$
$Y_1(t)$	$(r \times s)$
$X_{1a}(t)$	$(n \times r)$
$X_{1b}(t)$	$(n \times s)$
$Y_2(t)$	$(1 \times m)$
$X_{2a}(t)$	$(n \times 1)$
$X_{2b}(t)$	$(n \times m)$.

The matrices E, Q, and $P(t)$ must be symmetric. The function $F_i(t)$ is a term representing the forcing functions for the $X_i(t)$ differential

equations, and accordingly has dimension (n × p) for i = 1 and (n × q) for i = 2. For scalar control problems, the five types of differential equations become scalar differential equations. However, for multivariable control problems, $P(t)$ is always a square matrix; $X_i(t)$ (i=1,2) may represent either a matrix or a vector; and $Y_i(t)$ (i=1,2) may be either a matrix, vector, or scalar.

2.2.1   Solution for Type 1 Differential Equations

The Type 1 differential equations are defined by

$$\dot{P}(t) = - P(t)A - A^T P(t) + P(t)EP(t) - Q . \qquad (2.2.6)$$

The solution of the above differential matrix Riccati equation is well-known and, in fact, can be expressed in several different forms. One of the most useful forms of the solution is due to Potter [5,17,22,26-28], and is given by the sum of the steady-state solution (i.e. the solution to an algebraic Riccati equation) [1,5,17,22,25], and a transient term:

$$P(t) = P_{ss} + Z^{-1}(t) , \qquad (2.2.7)$$

where

$$0 = P_{ss}A + A^T P_{ss} - P_{ss}E P_{ss} + Q .$$

In order to obtain the differential equation for $Z(t)$, one needs the following expression for the derivative of a matrix inverse:

$$\frac{d}{dt}[Z^{-1}(t)] = - Z^{-1}(t)\dot{Z}(t)Z^{-1}(t). \qquad (2.2.8)$$

Substituting (2.2.7) into (2.2.6), and making use of (2.2.8), one obtains

$$\dot{Z}(t) = \bar{A}Z(t) + Z(t)\bar{A}^T - E , \qquad (2.2.9)$$

where

$$\bar{A} = A - EP_{ss}$$

is the closed-loop system dynamics matrix. The solution for $Z(t)$ can be cast in either of the following two forms [11,17,31]:

$$Z(t) = Z_{ss} + e^{\bar{A}(t-t_0)}[Z(t_0)-Z_{ss}]e^{\bar{A}^T(t-t_0)}, \quad Z(t_0) = [P(t_0)-P_{ss}]^{-1};$$

or

$$Z(t) = Z_{ss} + e^{-\bar{A}(t_f-t)}[Z(t_f)-Z_{ss}]e^{-\bar{A}^T(t_f-t)}, \quad Z(t_f) = [P(t_f)-P_{ss}]^{-1};$$

$$(2.2.10)$$

where Z_{ss} satisfies the algebraic Lyapunov equation [2,13,17,24]:

$$0 = \bar{A}Z_{ss} + Z_{ss}\bar{A}^T - E .$$

It can be shown that $Z(t)$ and $Z^{-1}(t)$ exist for well-posed optimal control problems.

As shown in Sections 2.2.2 - 2.2.5, the symmetric matrix $Z(t)$ plays a central role in the solution of differential equations of Types 2, 3, 4, and 5.

2.2.2   Solution for Type 2 Differential Equations

The Type 2 differential equations are characterized by differential equations with time-varying coefficient matrices, where the coefficient matrices are functionally dependent upon the Type 1 equations. The general form for the Type 2 equations is given by

$$\dot{X}_1(t) = -[A - EP(t)]^T X_1(t) + F_1(t) . \qquad (2.2.11)$$

On assuming a solution of the form

$$X_1(t) = Z^{-1}(t)W(t) , \qquad (2.2.12)$$

where $W(t)$ is unknown, it can be shown that the solution of (2.2.11) is given by [9]

$$X_1(t) = \Phi_1(t,t_o)X_1(t_o) + \int_{t_o}^{t} \Phi_1(t,\tau)F_1(\tau)d\tau , \qquad (2.2.13)$$

where

$$\Phi_1(t,t_o) = Z^{-1}(t)e^{\bar{A}(t-t_o)}Z(t_o)$$

is the state transition matrix for the homogeneous part of (2.2.11). The integral term in (2.2.13) is easily obtained when $F_1(t)$ can be expressed in terms of exponential matrices.

2.2.3   Solution for Type 3 Differential Equations

Like the Type 2 differential equations, the Type 3 differential equations are characterized by differential equations with time-varying coefficient matrices, where the coefficient matrices are functionally dependent on the Type 1 equations. The general form for the Type 3 equations is given by

$$\dot{X}_2(t) = [A - EP(t)]X_2(t) + F_2(t) . \qquad (2.2.14)$$

On assuming a solution of the form

$$X_2(t) = Z(t)W(t) ,$$

(2.2.15)

where $W(t)$ is unknown, it can be shown that the solution of (2.2.14) is given by

$$X_2(t) = \Phi_2(t,t_o)X_2(t_o) + \int_{t_o}^{t} \Phi_2(t,\tau)F_2(\tau)d\tau ,$$

(2.2.16)

where

$$\Phi_2(t,t_o) = Z(t)e^{-\bar{A}^T(t-t_o)}Z^{-1}(t_o)$$

is the state transition matrix for the homogeneous part of (2.2.14). The integral term in (2.2.16) can be easily evaluated when $F_2(t)$ is expressed in terms of products of $Z(t)$ and exponential matrices.

2.2.4 Solution for Type 4 Differential Equations

The Type 4 differential equations are characterized by products of Type 2 solutions. The general form for the Type 4 equation is given by

$$\dot{Y}_1(t) = X_{1a}^T(t)EX_{1b}(t) ,$$

(2.2.17)

where the equations for $X_{1a}(t)$ and $X_{1b}(t)$ are, in general, inhomogeneous:

$$\dot{X}_{1a}(t) = -[A - EP(t)]^T X_{1a}(t) + F_{1a}(t) ,$$

(2.2.18)

and

$$\dot{X}_{1b}(t) = -[A - EP(t)]^T X_{1b}(t) + F_{1b}(t) .$$

(2.2.19)

From Reference 9, the solution for $Y_1(t)$ is shown to be

$$Y_1(t) = X_{1a}^T(t)Z(t)X_{1b}(t) + Y_1(t_o) - X_{1a}^T(t_o)Z(t_o)X_{1b}(t_o)$$

$$- \int_{t_o}^t X_{1a}^T(\tau)Z(\tau)F_{1b}(\tau)d\tau - \int_{t_o}^t F_{1a}^T(\tau)Z(\tau)X_{1b}(\tau)d\tau \ .$$

$$(2.2.20)$$

The integral terms in (2.2.20) are easily computed when $F_{1a}(t)$ and $F_{1b}(t)$ are functions of exponential matrices.

2.2.5 Solutions for Type 5 Differential Equations

The Type 5 differential equations are characterized by products of Type 3 solutions and $Z^{-1}(t)$. The general form for the Type 5 equations is given by

$$\dot{Y}_2(t) = X_{2a}^T(t)Z^{-1}(t)EZ^{-1}(t)X_{2b}(t) \ , \qquad (2.2.21)$$

where the differential equations for $X_{2a}(t)$ and $X_{2b}(t)$ are, in general, inhomogeneous:

$$\dot{X}_{2a}(t) = [A - EP(t)]X_{2a}(t) + F_{2a}(t) \ , \qquad (2.2.22)$$

and

$$\dot{X}_{2b}(t) = [A - EP(t)]X_{2b}(t) + F_{2b}(t) \ . \qquad (2.2.23)$$

From Reference 9, the solution for $Y_2(t)$ is shown to be

$$Y_2(t) = - X_{2a}^T(t)Z^{-1}(t)X_{2b}(t) + Y_2(t_o) + X_{2a}^T(t_o)Z^{-1}(t_o)X_{2b}(t_o)$$

$$+ \int_{t_o}^t X_{2a}^T(\tau)Z^{-1}(\tau)F_{2b}(\tau)d\tau + \int_{t_o}^t F_{2a}^T(\tau)Z^{-1}(\tau)X_{2b}(\tau)d\tau \ .$$

$$(2.2.24)$$

The integral terms in (2.2.24) are easily computed when $F_{2a}(t)$ and $F_{2b}(t)$ can be expressed as products of $Z(t)$ and exponential matrices.

Throughout the developments of this section, one can observe the close relationship between equations of Type 2 and Type 3, and also between equations of Type 4 and Type 5. Indeed, this follows because equations of Type 2 and Type 3 are formal adjoints of one another.

Tables 2-1 and 2-2 provide a summary of the five basic differential equations and their solutions.

2.3   Example Applications of Closed-Form Solutions

Reference 9 presents solutions of three finite-time linear-quadratic optimal control problems using the closed-form solutions of Section 2.2. For comparison, alternative closed-form solutions based on the state transition matrix of the state-costate system are presented. The comparison of the amount of computational work required for each type of solution clearly demonstrates that the new class of solutions is more efficient.

In particular, using Potter's solution of Section 2.2.1, the propagation of the Riccati matrix is written as

$$P(t + \Delta t) = P_{ss} + Z^{-1}(t + \Delta t) , \qquad (2.3.1)$$

where $Z(t + \Delta t)$ is computed via

$$Z(t + \Delta t) = C + e^{\bar{A}\Delta t} Z(t) e^{\bar{A}^T \Delta t} , \quad C = Z_{ss} - e^{\bar{A}\Delta t} Z_{ss} e^{\bar{A}^T \Delta t} . \qquad (2.3.2)$$

Equation (2.3.2) requires roughly $3n^3/2$ flops for the propagation of the symmetric $Z(t)$ matrix. In computing the Riccati solution of (2.3.1), the symmetric definite matrix inversion requires $n^3/2$ flops. Thus, a total of $2n^3$ flops are required to propagate the Riccati solution over one time-step.

Table 2-1. Summary of Basic Differential Equations and Their Solutions

	Differential Equation	Solution
Type 1	$\dot{P}(t) = -P(t)A - A^T P(t) + P(t)EP(t) - Q$	$P(t) = P_{ss} + Z^{-1}(t)$
Type 2	$\dot{X}_1(t) = -[A - EP(t)]^T X_1(t) + F_1(t)$	$X_1(t) = \Phi_1(t,t_o)X_1(t_o) + \int_{t_o}^t \Phi_1(t,\tau)F_1(\tau)d\tau$
Type 3	$\dot{X}_2(t) = [A - EP(t)]X_2(t) + F_2(t)$	$X_2(t) = \Phi_2(t,t_o)X_2(t_o) + \int_{t_o}^t \Phi_2(t,\tau)F_2(\tau)d\tau$
Type 4	$\dot{Y}_1(t) = X_{1a}^T(t)EX_{1b}(t)$	$Y_1(t) = X_{1a}^T(t)Z(t)X_{1b}(t) + Y_1(t_o) - X_{1a}^T(t_o)Z(t_o)X_{1b}(t_o)$ $\quad - \int_{t_o}^t X_{1a}^T(\tau)Z(\tau)F_{1b}(\tau)d\tau - \int_{t_o}^t F_{1a}^T(\tau)Z(\tau)X_{1b}(\tau)d\tau$
Type 5	$\dot{Y}_2(t) = X_{2a}^T(t)Z^{-1}(t)EZ^{-1}(t)X_{2b}(t)$	$Y_2(t) = -X_{2a}^T(t)Z^{-1}(t)X_{2b}(t) + Y_2(t_o) + X_{2a}^T(t_o)Z^{-1}(t_o)X_{2b}(t_o)$ $\quad - \int_{t_o}^t X_{2a}^T(\tau)Z^{-1}(\tau)F_{2b}(\tau)d\tau + \int_{t_o}^t F_{2a}^T(\tau)Z^{-1}(\tau)X_{2b}(\tau)d\tau$

Table 2-2. Summary of Auxiliary Differential Equations and Their Solutions

Differential Equation	Solution
$\dot{z}(t) = \bar{A}z(t) + z(t)\bar{A}^T - E$ $\bar{A} = A - EP_{ss}$ $z(t_o) = [P(t_o) - P_{ss}]^{-1}, \quad z(t_f) = [P(t_f) - P_{ss}]^{-1}$	$z(t) = z_{ss} + e^{\bar{A}(t-t_o)}[z(t_o) - z_{ss}]e^{\bar{A}^T(t-t_o)}$ $\quad\quad = z_{ss} + e^{-\bar{A}(t_f-t)}[z(t_f) - z_{ss}]e^{-\bar{A}^T(t_f-t)}$
$\dfrac{d}{dt}[\Phi_1(t,t_o)] = -[A - EP(t)]^T\Phi_1(t,t_o)$ $\Phi_1(t_o,t_o) = I$	$\Phi_1(t,t_o) = z^{-1}(t)e^{\bar{A}(t-t_o)}z(t_o)$
$\dfrac{d}{dt}[\Phi_2(t,t_o)] = [A - EP(t)]\Phi_2(t,t_o)$ $\Phi_2(t_o,t_o) = I$	$\Phi_2(t,t_o) = z(t)e^{-\bar{A}^T(t-t_o)}z^{-1}(t_o)$

An alternative way of computing the matrix Riccati solution is the well-known Kalman-Englar method [18], where $P(t)$ is propagated at intervals of Δt by

$$P(t+\Delta t) = [\Theta_{21}(t+\Delta t,t) + \Theta_{22}(t+\Delta t,t)P(t)][\Theta_{11}(t+\Delta t,t) + \Theta_{12}(t+\Delta t,t)P(t)]^{-1},$$

$$(2.3.3)$$

where $\Theta_{ij}(t+\Delta t,t)$ are partitions of the transition matrix for the state-costate system; that is,

$$\Theta(t + \Delta t,t) = \Theta(\Delta t) = e^{\Omega \Delta t} \qquad (2.3.4)$$

and

$$\Omega = \begin{bmatrix} A & -E \\ -Q & -A^T \end{bmatrix}.$$

For linear time-invariant systems, Θ is only a function of Δt, and hence need only be computed once.

The number of operations required for the propagation of $P(t)$ via (2.3.3) is n^3 flops for each of the $\Theta_{22}P$ and $\Theta_{12}P$ products, $n^3/3$ flops for the L-U decomposition (with partial pivoting) of the $[\Theta_{11} + \Theta_{12}P]$ term, $n^3/2$ for forward elimination, and $n^3/6$ for back-substitution, where symmetry of $P(t)$ is taken into account. The total number of operations adds up to about $3n^3$ flops. Thus, the Kalman-Englar method requires about 50% more operations than Potter's method for propagating $P(t)$ at intervals of Δt. Moreover, numerical difficulties arise in the Kalman-Englar method when Δt is chosen too large, causing the term to be inverted to be nearly singular [21]. For the propagation based on Potter's solution, such difficulties do not occur. Another solution approach is the negative exponential solution derived by Vaughan [38], which produces a numerically stable algorithm. However, since this method involves complex eigenvectors of the Hamiltonian matrix, the use of complex arithmetic causes the

operation count to be many times higher than that for the Kalman-Englar method.

Table 2-3 summarizes the solutions for state and control trajectories of the three example problems presented in Reference 9, which include the optimal linear regulator, the controller with terminal constraints, and the tracking/disturbance accommodating controller. A remarkable fact is that despite the differences between the three control problems, the state and control trajectories may be cast into the same general form, namely,

$$x(t) = Z_{ss}a(t) + b(t) , \qquad\qquad (2.3.5)$$

and

$$u(t) = - D_1 a(t) - D_2 b(t) , \qquad\qquad (2.3.6)$$

where

$$D_1 = R^{-1}B^T[P_{ss}Z_{ss} + I] ,$$

and

$$D_2 = R^{-1}B^T P_{ss} .$$

The definitions of a(t) and b(t) , however, are slightly different for each problem.

2.4   Subspace Reduction for the Hamiltonian Matrix

It can be shown that the new class of solutions, which involves the variables P_{ss}, Z_{ss}, $e^{\bar{A}t}$, and $e^{-\bar{A}^T t}$, are related to the closed-form solutions involving partitions of the state transition matrix by means of reducing subspace transformations of the Hamiltonian matrix:

Table 2-3. Summary of Example Applications of Closed-Form Solutions

Type of Controller	Optimal Linear Regulator	Controller with Terminal Constraints	Tracking/Disturbance Accommodating Controller
Performance Index	$J = \frac{1}{2}\lVert y(t_f)\rVert^2_{P'}$ $+ \frac{1}{2}\int_{t_o}^{t_f}[\lVert y(t)\rVert^2_{Q'} + \lVert u(t)\rVert^2_R]dt$	$J = \frac{1}{2}\lVert y(t_f)\rVert^2_{P'}$ $+ \frac{1}{2}\int_{t_o}^{t_f}[\lVert y(t)\rVert^2_{Q'} + \lVert u(t)\rVert^2_R]dt$	$J = \frac{1}{2}\lVert y^*(t_f) - y(t_f)\rVert^2_{P'}$ $+ \frac{1}{2}\int_{t_o}^{t_f}[\lVert y^*(t) - y(t)\rVert^2_{Q'} + \lVert u(t)\rVert^2_R]dt$
Necessary Conditions	$\dot{x}(t) = Ax(t) + Bu(t)$, x_o given $\dot{\lambda}(t) = -Qx(t) - A^T\lambda(t)$, $\lambda(t_f) = P_f x(t_f)$ $u(t) = -R^{-1}B^T\lambda(t)$	$\dot{x}(t) = Ax(t) + Bu(t)$, x_o given $\dot{\lambda}(t) = -Qx(t) - A^T\lambda(t)$, $\lambda(t_f) = C^T M^T \nu + P_f x(t_f)$ $u(t) = -R^{-1}B^T\lambda(t)$ $\psi(t_f) = Mx(t_f) - \psi_d = 0$	$\dot{x}(t) = Ax(t) + Bu(t) + \Lambda B(t)$, x_o given $\dot{\lambda}(t) = -Qx(t) + \tilde{Q}H_x s(t) - A^T\lambda(t)$ $\lambda(t_f) = P_f x(t_f) - \tilde{P}_f H_x s(t_f)$ $u(t) = -R^{-1}B^T\lambda(t)$
Feedback Form	$\lambda(t) = P(t)x(t)$	$\lambda(t) = P(t)x(t) - S(t)\psi_d$	$\lambda(t) = P(t)x(t) - \xi(t)$
Sweep Variables	$\dot{P} = -PA - A^T P + PEP - Q$ $P(t_f) = P_f$	$\dot{P} = -PA - A^T P + PEP - Q$, $P(t_f) = \bar{P} - \bar{S}G^{-1}\bar{S}^T$ $\dot{S} = -[A - EP]^T S$, $S(t_f) = -\bar{S}G^{-1}$	$\dot{P} = -PA - A^T P + PEP - Q$, $P(t_f) = P_f$ $\dot{\xi} = -[A - EP]^T\xi - \tilde{Q}H_x s + PAB$, $\xi(t_f) = \tilde{P}_f H_x s(t_f)$
State Trajectory	$x(t) = z_{ss}a(t) + b(t)$	$x(t) = z_{ss}a(t) + b(t)$	$x(t) = z_{ss}a(t) + b(t)$
Control Trajectory	$u(t) = -D_1 a(t) - D_2 b(t)$	$u(t) = -D_1 a(t) - D_2 b(t)$	$u(t) = -D_1 a(t) - D_2 b(t)$

Table 2-3. Summary of Example Applications of Closed-Form Solutions (Continued)

Expression for a(t)	$a(t) = e^{-\bar{A}^T(t-t_o)} z^{-1}(t_o) x_o$	$a(t) = e^{-\bar{A}^T(t-t_o)}[z^{-1}(t_o)x_o - s(t_o)\psi_d]$	$a(t) = e^{-\bar{A}^T(t-t_o)}[z^{-1}(t_o)x_o - \xi(t_o)]$ $+ G(-\bar{A}^T, K_2, \Omega, t, t_o)s_o$ $- G(-\bar{A}^T, K_4, L, t, t_o)\beta_o$
Expression for b(t)	$b(t) = e^{\bar{A}(t-t_o)}[z(t_o) - z_{ss}]$ $\times z^{-1}(t_o)x_o$	$b(t) = e^{\bar{A}(t-t_o)}$ $\times [x_o - z_{ss}(z^{-1}(t_o)x_o - s(t_o)\psi_d)]$	$b(t) = e^{\bar{A}(t-t_o)}[x_o - z_{ss}(z^{-1}(t_o)x_o - \xi(t_o))]$ $- G(\bar{A}, K_1, \Omega, t, t_o)s_o$ $+ G(\bar{A}, K_3, L, t, t_o)\beta_o$
Recursion for a(t)	$a(t + \Delta t) = e^{-\bar{A}^T \Delta t} a(t)$	$a(t + \Delta t) = e^{-\bar{A}^T \Delta t} a(t)$	$a(t + \Delta t) = e^{-\bar{A}^T \Delta t} a(t) + C_2 s(t) - C_4 \beta(t)$
Recursion for b(t)	$b(t + \Delta t) = e^{\bar{A}\Delta t} b(t)$	$b(t + \Delta t) = e^{\bar{A}\Delta t} b(t)$	$b(t + \Delta t) = e^{\bar{A}\Delta t} b(t) - C_1 s(t) + C_3 \beta(t)$
Work for x(t) and u(t) propagation (flops)	$3n^2 + 2pn$	$3n^2 + 2pn$	$3n^2 + 2pn + 4n_o^2 + n_d^2 + 4nn_o + 2nn_d$
Work for transition matrix solution to x(t) and u(t) (flops)	$4n^2 + pn$	$4n^2 + pn$	$4n^2 + pn + 4n_o^2 + n_d^2 + 4nn_o + 2nn_d$

$$\begin{bmatrix} A & -E \\ -Q & -A^T \end{bmatrix} = \begin{bmatrix} I & Z_{ss} \\ P_{ss} & P_{ss}Z_{ss}+I \end{bmatrix} \begin{bmatrix} \bar{A} & 0 \\ 0 & -\bar{A}^T \end{bmatrix} \begin{bmatrix} I+Z_{ss}P_{ss} & -Z_{ss} \\ -P_{ss} & I \end{bmatrix}.$$

$$(2.4.1)$$

In (2.4.1), the left hand side represents the Hamiltonian matrix, Ω, of (2.3.4). Exponentiation of (2.4.1) leads to the following block-diagonalizing transformation for the state transition matrix:

$$\begin{bmatrix} \Theta_{11} & \Theta_{12} \\ \Theta_{21} & \Theta_{22} \end{bmatrix} = \begin{bmatrix} I & Z_{ss} \\ P_{ss} & P_{ss}Z_{ss}+I \end{bmatrix} \begin{bmatrix} e^{\bar{A}(t-t_o)} & 0 \\ 0 & e^{-\bar{A}^T(t-t_o)} \end{bmatrix}$$

$$\times \begin{bmatrix} I+Z_{ss}P_{ss} & -Z_{ss} \\ -P_{ss} & I \end{bmatrix}, \qquad (2.4.2)$$

where $\Theta_{ij} = \Theta_{ij}(t,t_o)$ are partitions of the state transition matrix

$$\Theta(t,t_o) = e^{\Omega(t-t_o)}. \qquad (2.4.3)$$

SECTION 3

SPACECRAFT SLEWING MANEUVERS USING A CLOSED-FORM SOLUTION
FOR THE NEIGHBORING EXTREMAL PATH PROBLEM

3.1   Introduction

The optimal control problem in this section is specified by defining a performance index which consists of a penalty on elapsed time, a quadratic penalty on the terminal states and controls, and an integral of quadratic penalties on the states, controls, and control rates. The final time is free, and specified terminal constraints produce a terminal manifold which also may be a function of the final time. Assuming that the nominal control and state trajectories are known, one seeks the perturbation feedback gains which cause the system to follow a neighboring extremal path when subjected to small perturbations in the initial conditions and terminal constraints. Necessary conditions for the perturbed system are stated, and the solution for the nominal trajectory is shown. Solutions for the perturbation feedback gains are developed based on the results of Section 2. Perfect plant knowledge and perfect state estimation is assumed. A time-to-go indexing scheme is used for applying the feedback gains so that the controller does not run out of feedback gains if the actual final time is longer than the nominal final time. Slight numerical modifications are presented for overcoming the numerical sensitivities of this type of controller. Two retargeting example maneuvers are shown, involving a spacecraft model consisting of a rigid body with four flexible appendages. An extension is proposed for using the closed-form solutions in control problems involving nonlinear systems by linearizing the nonlinear plant equations about the nominal trajectory.

3.2   Statement of the Control Problem

Let us assume that we have obtained the p-dimensional nominal control vector $u^N(t)$, which minimizes the quadratic performance index

$$J = W_t t_f + \frac{1}{2} x_f^T S_f x_f + \frac{1}{2} \int_{t_o}^{t_f} [x^T W_{xx} x + u^T W_{uu} u] dt \ , \qquad (3.2.1)$$

subject to

$$\dot{x} = Ax + Bu \ , \quad x(t_o) = x_o \text{ given} \ , \qquad (3.2.2)$$

$$\psi[x(t_f), t_f] = Mx(t_f) - \psi_d^N(t_f) = 0 \ , \quad \text{and } t_f \text{ unspecified} \ . \qquad (3.2.3)$$

In the above equations, x is the n-dimensional state vector, A and B are the time-invariant state dynamics and control influence matrices, ψ is a q-dimensional vector of terminal constraints, $S_f = S_f^T \geq 0$ and $W_{xx} = W_{xx}^T \geq 0$ are weighting matrices for the state, $W_{uu} = W_{uu}^T > 0$ is a weighting matrix for the control, and $W_t \geq 0$ is a weight for the final time. The following necessary conditions must be satisfied by the nominal optimal control and state trajectories [7]:

$$\dot{x} = Ax + Bu \ , \quad x(t_o) \text{ given} \ , \qquad (3.2.4)$$

$$\dot{\lambda} = -W_{xx} x - A^T \lambda \ , \quad \lambda(t_f) = S_f x(t_f) + M^T \nu \ , \qquad (3.2.5)$$

$$u = -W_{uu}^{-1} B^T \lambda \ , \qquad (3.2.6)$$

$$\psi[x(t_f), t_f] = 0 \ , \qquad (3.2.7)$$

$$\Omega = \frac{d\Phi}{dt}\Big|_{t_f} + \frac{1}{2} [x^T W_{xx} x + u^T W_{uu} u]\Big|_{t_f} = 0 \ , \qquad (3.2.8)$$

where

$$\Phi = W_t t_f + \frac{1}{2} x_f^T S_f x_f + \nu^T \psi ,$$

$$\frac{d\Phi}{dt} = W_t - \nu^T \psi_d^N(t_f) + [x_f^T S_f + \nu^T M] \dot{x}_f ,$$

$\lambda(t)$ is the n-dimensional costate vector, and ν is the q-dimensional vector of Lagrange multipliers for the terminal constraints.

Let us now consider small perturbations in the initial states $\delta x(t_o)$, and in the terminal constraints $d\psi$. The perturbation problem is then to seek the the correction to the control, $\delta u(t)$, which causes the perturbed system to minimize the original performance index subject to the new initial conditions and new final constraints. Moreover, we seek a feedback form for the solution of $\delta u(t)$, which involves the perturbations in the state, $\delta x(t)$, and the perturbations in the final conditions $d\psi$. The necessary conditions which must be satisfied by the perturbed system are given by the following equations [7]:

$$\delta \dot{x} = A\delta x + B\delta u, \quad \delta x(t_o) \text{ given} , \tag{3.2.9}$$

$$\delta \dot{\lambda} = - W_{xx} \delta x - A^T \delta \lambda , \tag{3.2.10}$$

$$\delta u = - W_{uu}^{-1} B^T \delta \lambda , \tag{3.2.11}$$

$$\delta \lambda(t_f) = [\frac{\partial^2 \Phi}{\partial x^2}]\big|_{t_f} \delta x_f + [\frac{\partial \psi}{\partial x}]\big|_{t_f}^T d\nu + [\frac{\partial \Omega}{\partial x}]\big|_{t_f}^T dt_f$$

$$= S_f \delta x + M^T d\nu + [S_f \dot{x}_f + A^T S_f x_f + A^T M^T \nu + W_{xx} x_f] dt_f , \tag{3.2.12}$$

$$d\psi = [\frac{\partial \psi}{\partial x}]\big|_{t_f} \delta x_f + [\frac{d\psi}{dt}]\big|_{t_f}^T dt_f = M\delta x_f + [M\dot{x}_f - \psi_d^N(t_f)] dt_f ,$$

$$\tag{3.2.13}$$

-20-

and

$$d\Omega = [\frac{\partial\Omega}{\partial x}]|_{t_f} \delta x_f + [\frac{d\psi}{dt}]|_{t_f}^T d\nu + [\frac{d\Omega}{dt}]|_{t_f} dt_f = 0$$

$$= [\dot{x}_f^T S_f + x_f^T S_f A + \nu^T MA + x_f^T W_{xx}]\delta x_f + [M\dot{x}_f - \psi_d^N(t_f)]^T d\nu$$

$$+ [-\nu^T \ddot{\psi}_d(t_f) + (\dot{x}_f^T S_f + x_f^T S_f A + \nu^T MA + x_f^T W_{xx})\dot{x}_f]dt_f .$$

(3.2.14)

3.3 Solution for the Nominal Trajectory

The solution for the nominal trajectory may be obtained by using the state transition matrix and an exponential form for J. For a given final time t_f, the final states and costates can be written as

$$\left\{ \begin{array}{c} x(t_f) \\ \lambda(t_f) \end{array} \right\} = [e^{G(t_f - t_o)}] \left\{ \begin{array}{c} x(t_o) \\ \lambda(t_o) \end{array} \right\} ,$$

(3.3.1)

where

$$G = \left[\begin{array}{cc} A & -BW_{uu}^{-1}B^T \\ -W_{xx} & -A^T \end{array} \right] ,$$

and

$$e^{G(t_f - t_o)} = \left[\begin{array}{cc} \Phi_{xx} & \Phi_{x\lambda} \\ \Phi_{\lambda x} & \Phi_{\lambda\lambda} \end{array} \right]$$

is the state transition matrix for $t = t_f$. By introducing the terminal constraint of (3.2.3) into (3.3.1), and using the boundary condition of (3.2.5), one obtains

$$
\begin{bmatrix} I & 0 \\ S_f & M^T \\ M & 0 \end{bmatrix} \left\{ \begin{array}{c} x(t_f) \\ \nu \end{array} \right\} = \begin{bmatrix} \Phi_{xx} & \Phi_{x\lambda} \\ \Phi_{\lambda x} & \Phi_{\lambda\lambda} \\ 0 & 0 \end{bmatrix} \left\{ \begin{array}{c} x(t_o) \\ \lambda(t_o) \end{array} \right\} + \left\{ \begin{array}{c} 0 \\ 0 \\ \psi_d^N(t_f) \end{array} \right\} .
$$

$$(3.3.2)$$

Upon rearranging and placing the unknown variables on the left hand side, one obtains

$$
\begin{bmatrix} I & 0 & -\Phi_{x\lambda} \\ S_f & M^T & -\Phi_{\lambda\lambda} \\ M & 0 & 0 \end{bmatrix} \left\{ \begin{array}{c} x(t_f) \\ \nu \\ \lambda(t_o) \end{array} \right\} = \begin{bmatrix} \Phi_{xx} & 0 \\ \Phi_{\lambda x} & 0 \\ 0 & I \end{bmatrix} \left\{ \begin{array}{c} x(t_o) \\ \psi_d^N(t_f) \end{array} \right\} , (3.3.3)
$$

from which $x(t_f)$, ν, and $\lambda(t_o)$ may be obtained via Gaussian elimination.

The above solution assumes that t_f is known. However, for a free-final-time problem, the optimality condition, $\Omega = 0$, of (3.2.8) must be satisfied as well. This conditon produces a local minimum for J. To obtain the global minimum, one can numerically compute the value of J over a reasonable range of t_f and find which value of t_f produces the lowest value of J. Efficient propagation algorithms for J are presented in Reference 9 for computing values of J for different final times.

Using (3.2.1), (3.2.8), (3.3.3), and the propagation equations for J, one can numerically compute values of J and Ω over a range of final times, and hence find the optimal t_f. For the case where one wishes to adjust W_t so that the optimal final time is at a desired value, one merely computes Ω using (3.2.8) and (3.3.3) at the desired final time and obtain the required value of W_t to make $\Omega = 0$.

Having found the values of the optimal final time and initial costates, the nominal state and control trajectories are given by

$$x^N(t) = [I \; 0]e^{G(t-t_o)} \left\{ \begin{array}{c} x(t_o) \\ \lambda(t_o) \end{array} \right\} , \qquad (3.3.4)$$

and

$$u^N(t) = - W_{uu}^{-1}B^T[0 \; I]e^{G(t-t_o)} \left\{ \begin{array}{c} x(t_o) \\ \lambda(t_o) \end{array} \right\} . \qquad (3.3.5)$$

3.4   Solution for the Feedback Gains

We now seek the solution for $\delta u(t)$ in the form

$$\delta u(t) = - K_1(t)\delta x(t) - K_2(t)d\psi , \qquad (3.4.1)$$

where

$$u(t) = u^N(t) + \delta u(t) ,$$

$$\delta x(t) = x^N(t) - x(t) ,$$

K_1 and K_2 are the required feedback gains, and $u(t)$ and $x(t)$ are the perturbed controls and states. By manipulating the terminal conditions of (3.2.12) through (3.2.14) into the following form, which is assumed to be valid for $t_o \leq t \leq t_f$, the costate perturbations are expressed in a feedback form which leads to (3.4.1):

$$\left\{ \begin{array}{c} \delta\lambda(t) \\ d\nu \\ dt_f \end{array} \right\} = \left[\begin{array}{ccc} \hat{S}(t) & \hat{R}(t) & \hat{m}(t) \\ \hat{R}^T(t) & \hat{Q}(t) & \hat{n}(t) \\ \hat{m}^T(t) & \hat{n}^T(t) & \hat{\alpha}(t) \end{array} \right] \left\{ \begin{array}{c} \delta x(t) \\ -d\psi \\ -d\Omega = 0 \end{array} \right\} , \qquad (3.4.2)$$

where

$$\hat{S}(t_f) = \bar{S} - \bar{R}\bar{Q}^{-1}\bar{R}^T \, , \quad \hat{R}(t_f) = -\bar{R}\bar{Q}^{-1} \, , \quad \hat{m}(t_f) = \bar{R}\bar{Q}^{-1}\bar{n} - \bar{m} \, ,$$

$$\hat{Q}(t_f) = -\bar{Q}^{-1} \, , \quad \hat{n}(t_f) = \bar{Q}^{-1}\bar{n} \, , \quad \hat{\alpha}(t_f) = -\bar{n}^T\bar{Q}^{-1}\bar{n} - \bar{\alpha} \, ,$$

$$\bar{S} = S - \frac{mm^T}{\alpha} \, , \quad \bar{R} = R - \frac{mn^T}{\alpha} \, , \quad \bar{m} = \frac{m}{\alpha} \, ,$$

$$\bar{Q} = Q - \frac{nn^T}{\alpha} \, , \quad \bar{n} = \frac{n}{\alpha} \, , \quad \bar{\alpha} = \frac{1}{\alpha} \, ,$$

$$S = \left[\frac{\partial^2\phi}{\partial x^2}\right]\Big|_{t_f} \, , \quad R = \left[\frac{\partial\psi}{\partial x}\right]^T\Big|_{t_f} \, , \quad m = \left[\frac{\partial\Omega}{\partial x}\right]^T\Big|_{t_f} \, ,$$

and

$$Q = 0 \, , \quad n = \left[\frac{d\psi}{dt}\right]\Big|_{t_f} \, , \quad \alpha = \left[\frac{d\Omega}{dt}\right]\Big|_{t_f} \, .$$

Notice that $\bar{Q}$ is singular because $Q = 0$.

Treating $d\nu$, dt_f, $d\psi$, and $d\Omega$ as constants, one can differentiate (3.4.2) using (3.2.9) through (3.2.11) and collect terms to obtain the differential equations for the coefficient matrices:

$$\dot{\hat{S}} = -\hat{S}A - A^T\hat{S} + \hat{S}E\hat{S} - W_{xx} \, , \tag{3.4.3}$$

$$\dot{\hat{R}} = -[A - E\hat{S}]^T\hat{R} \, , \tag{3.4.4}$$

$$\dot{\hat{m}} = -[A - E\hat{S}]^T\hat{m} \, , \tag{3.4.5}$$

$$\dot{\hat{Q}} = \hat{R}^T E\hat{R} \, , \tag{3.4.6}$$

$$\dot{\hat{n}} = \hat{R}^T E\hat{m} \, , \tag{3.4.7}$$

$$\dot{\hat{\alpha}} = \hat{m}^T E\hat{m} \, , \tag{3.4.8}$$

where

$$E = BW_{uu}^{-1}B^T .$$

The matrices $\hat{S}(t)$ and $\hat{R}(t)$ are used for the perturbation feedback, while the vectors $\hat{m}(t)$ and $\hat{n}(t)$ are used for the estimation of the change in the final time. The matrix $\hat{Q}(t)$ and the scalar $\hat{\alpha}(t)$ are not needed for solving the control problem.

The solution of the Type 1 differential Riccati equation for $\hat{S}(t)$ is shown in Section 2.2.1 to be

$$\hat{S}(t) = \hat{S}_{ss} + Z^{-1}(t) , \qquad (3.4.9)$$

where $\hat{S}_{ss}$ satisfies the steady-state Riccati equation

$$0 = -\hat{S}_{ss}A - A^T\hat{S}_{ss} + \hat{S}E\hat{S} - W_{xx} .$$

From Table 2-2, the solution for $Z(t)$ can be shown to be

$$Z(t) = Z_{ss} + e^{\bar{A}(t-t_o)}[Z(t_o) - Z_{ss}]e^{\bar{A}^T(t-t_o)} , \qquad (3.4.10)$$

where $\bar{A} = A - E\hat{S}_{ss}$ and Z_{ss} satisfies the steady-state Lyapunov equation for $Z(t)$ defined following (2.2.10). Since $\hat{R}(t)$ and $\hat{m}(t)$ satisfy differential equations of Type 2, their solutions are given by (see Tables 2-1 and 2-2):

$$\hat{R}(t) = Z^{-1}(t)e^{\bar{A}(t-t_o)}Z(t_o)\hat{R}(t_o) , \qquad (3.4.11)$$

and

$$\hat{m}(t) = Z^{-1}(t)e^{\bar{A}(t-t_o)}Z(t_o)\hat{m}(t_o) . \qquad (3.4.12)$$

Since $\hat{n}(t)$ satisfies a differential equation of Type 4, its solution is obtained from Table 2-1 as

$$\hat{n}(t) = \hat{R}^T(t)Z(t)\hat{m}(t) + \hat{n}(t_o) - \hat{R}^T(t_o)Z(t_o)\hat{m}(t_o) . \qquad (3.4.13)$$

The initial conditions for $\hat{S}(t)$, $\hat{R}(t)$, $\hat{m}(t)$, and $\hat{n}(t)$ are required for propagating the feedback gains forward in time; these are listed in Reference 9.

Using (3.2.11) and (3.4.2), one can write the feedback gains of (3.4.1) as

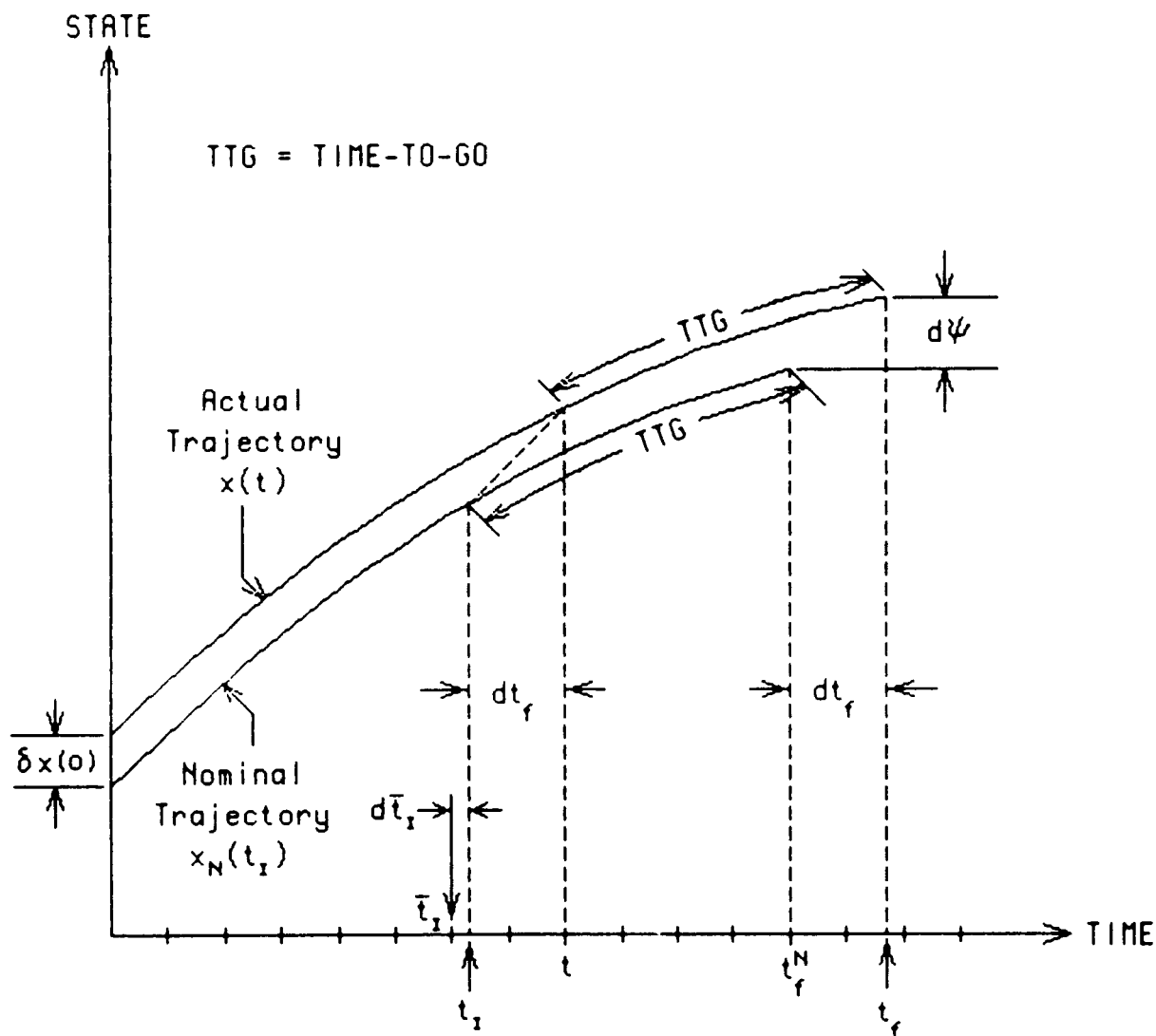$$K_1(t) = W_{uu}^{-1}B^T\hat{S}(t) , \qquad (3.4.14)$$

and

$$K_2(t) = - W_{uu}^{-1}B^T\hat{R}(t) , \qquad (3.4.15)$$

where the solutions of $\hat{S}(t)$ and $\hat{R}(t)$ are given by (3.4.9) and (3.4.11), respectively.

3.5 Time-To-Go Indexing Scheme

On observing the time arguments in (3.4.1) and recalling the fact that the final time is free, it quickly becomes apparent that if the optimal final time of the perturbed system lies beyond the nominal final time, then the feedback gains are undefined for part of the time ($t > t_f^N$) along the neighboring extremal path. One of the methods suggested for eliminating this problem is the use of time-to-go indexing [3,20,33] so that the time-to-go on the perturbed trajectory is the same as the time-to-go on the nominal trajectory (see Figure 3-1). Equation (3.4.1) is then re-written as

$$\delta u(t) = - K_1(t_I)\delta x(t) - K_2(t_I)d\psi , \qquad (3.5.1)$$

STATE

TTG = TIME-TO-GO

Actual
Trajectory
x(t)

Nominal
Trajectory
$x_N(t_I)$

$\delta x(o)$

$d\bar{t}_I$

$\bar{t}_I$

dt_f

dt_f

$d\psi$

TTG

TTG

TIME

t_I

t

t_f^N

t_f

t = Current Time t_I = Indexed Time

t_f^N = Nominal Final Time t_f = Actual Final Time

$\bar{t}_I$ = Time-points at which Gains are Computed

Figure 3-1. Time-To-Go Indexing Scheme

where

$$t_f^N - t_I = t_f - t ,$$

$$dt_f = t - t_I = t_f - t_f^N ,$$

t is the current time, t_I is the indexed time, t_f^N is the nominal final time, and t_f is the final time on the perturbed trajectory.

To compute the indexed time, let us re-write the last row of (3.4.2) for the change in final time:

$$dt_f = \hat{m}^T(t_I)\delta x(t) - \hat{n}^T(t_I)d\psi , \qquad (3.5.2)$$

where the time arguments for $\hat{m}^T(t)$ and $\hat{n}^T(t)$ have been changed to t_I. Since the feedback gains $\hat{S}(t)$, $\hat{R}(t)$, $\hat{m}(t)$, and $\hat{n}(t)$ are efficiently propagated at fixed time intervals, let us define $\bar{t}_I$ as the points in time at which the values of the feedback gains are available:

$$\bar{t}_I = n\Delta t, \quad n = 1,2,3, \ldots \qquad (3.5.3)$$

where Δt is the propagation time step. On assuming that the perturbed terminal manifold is given by

$$Mx(t_f) = \psi_d(t_f) , \qquad (3.5.4)$$

the vector $d\psi$ of (3.5.2) is computed via

$$d\psi = \psi_d(t_f) - \psi_d^N(t_f). \qquad (3.5.5)$$

Since t_f of (3.5.5) depends on the value of dt_f, (3.5.2) represents an implicit equation for dt_f.

To interpolate the gains to the indexed time, we define

$$d\bar{t}_I = t_I - \bar{t}_I \, , \qquad\qquad\qquad (3.5.6)$$

where $\bar{t}_I$ is a discrete time-point which is close to t_I, so that $d\bar{t}_I$ is smaller than Δt in magnitude. The local quadratic fit for a generic variable $V(t_I)$ is then given by [9]

$$V_{ij}(t_I) = \frac{1}{2}(d^2-d)V_{ij}(\bar{t}_I - \Delta t) + (1-d^2)V_{ij}(\bar{t}_I)$$

$$+ \frac{1}{2}(d^2+d)V_{ij}(\bar{t}_I + \Delta t) \, , \qquad\qquad (3.5.7)$$

where

$$d = d\bar{t}_I / \Delta t \, ,$$

and V_{ij} may represent an element of either $\hat{S}$, $\hat{R}$, $\hat{m}$, or $\hat{n}$.

The solution for the indexed time is obtained by guessing a value for $d\bar{t}_I$, computing the error in satisfying (3.5.2) via

$$\varepsilon = \hat{m}^T(t_I)\delta x(t) - \hat{n}^T(t_I)d\psi - t + \bar{t}_I + d\bar{t}_I \, , \qquad (3.5.8)$$

and updating the value of $d\bar{t}_I$ via

$$d\bar{t}_I \;:=\; d\bar{t}_I - \varepsilon. \qquad\qquad\qquad (3.5.9)$$

Equations (3.5.8) and (3.5.9) are iteratively applied [33] until the value of $d\bar{t}_I$ converges. The previously converged value of $d\bar{t}_I$ is used as the starting guess in the iteration.

The logic for propagating the gains is as follows. If $d\bar{t}_I > \Delta t$, then $\bar{t}_I$ is incremented by Δt, and the gains are propagated forward by one time-step. If $d\bar{t}_I < -\Delta t$, then $\bar{t}_I$ is decremented by Δt, and the gains are propagated backwards by one time-step. The above propagation is repeated, if necessary, until $|d\bar{t}_I| < \Delta t$. When $\bar{t}_I$ is incremented until $\bar{t}_I = t_f^N$, then the end of the maneuver is reached. Backward propagation of the gains, though not occuring often, may be needed when there are

disturbances acting on the system, or when there is a sudden change in the terminal manifold during the control interval. Figure 3-2 shows the block diagram for the free-final-time perturbation feedback controller.

3.6   Illustrative Examples

The specific model considered in this section consists of a rigid hub with four identical elastic appendages attached symmetrically about the central hub, and is derived from the experimental structure of [6], using NASTRAN data (see Fig. 3-3). In particular, the following idealizations are considered: (i) single-axis maneuvers, (ii) in-plane motion, (iii) antisymmetric deformations, (iv) small linear flexural deformations, (v) only the linear time-invariant form of the equations of motion are considered, and (vi) the control actuator is modeled as a concentrated torque generating device. Figure 3-4 shows the first three antisymmetric modes, which, with the rigid body mode, defines the full-order model. The control system for the vehicle consists of a single controller in the rigid part of the structure. The structural parameters of the model are presented in [6]. Because of the above assumptions, only the antisymmetric modes are used for the example cases in this section. In addition, full state feedback is assumed.

The rigid body mode and the first elastic mode are chosen for inclusion in the state vector for the control problem. Hence, the second and third elastic modes represent residual modes. Control smoothing is done by penalizing the first and second time derivatives of the control in the performance index, and augmenting the state vector with the control and its first time derivative. The state vector is given by

$$x = [\eta_0 \; \eta_1 \; \dot{\eta}_0 \; \dot{\eta}_1 \; u \; \dot{u}]^T,$$ (3.6.1)

where η_0 and η_1 are the amplitudes of the rigid mode and first elastic mode, and u is the control torque.
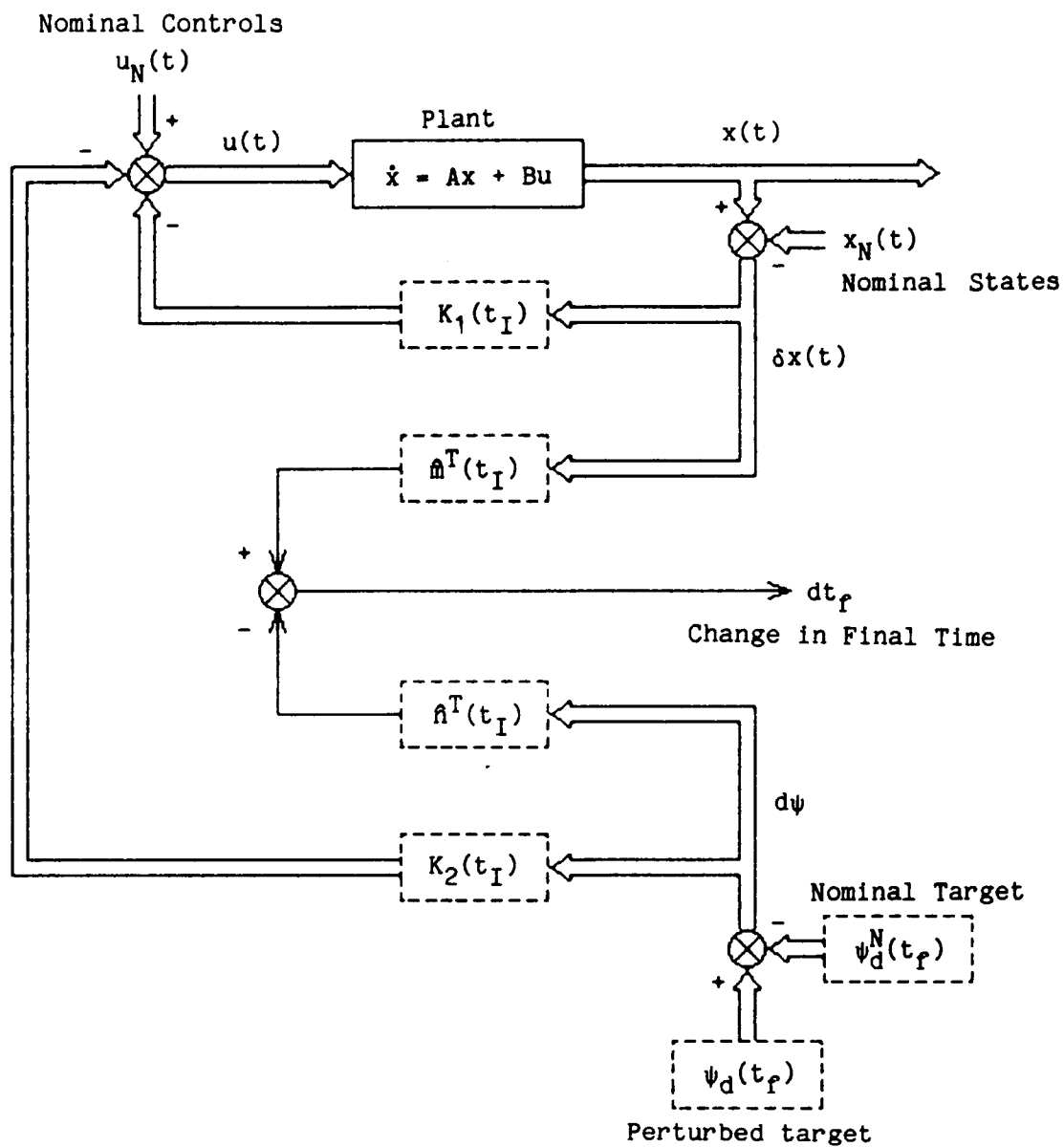
Figure 3-2.   Block Diagram for the Free-Final-Time Perturbation
             Feedback Controller

Dashed lines indicate variables which
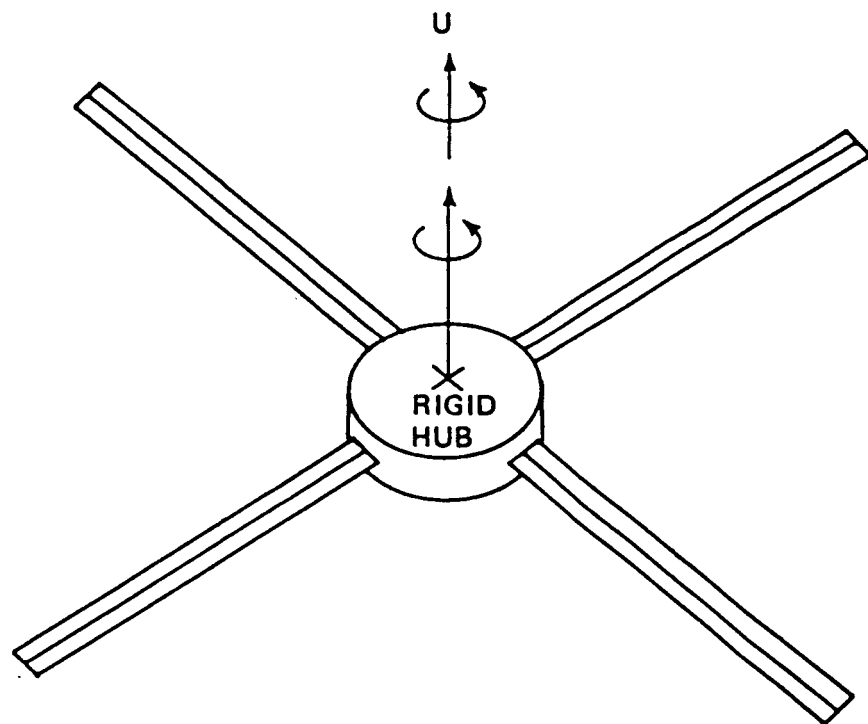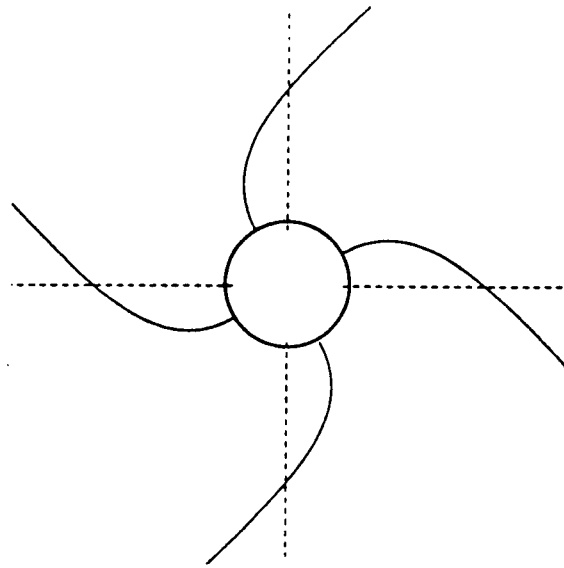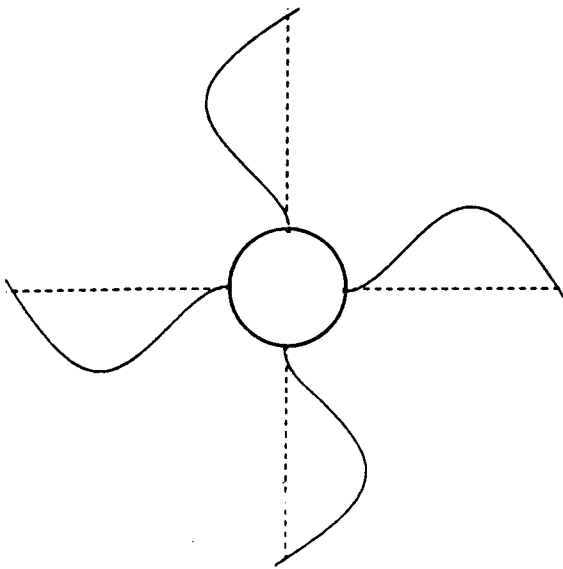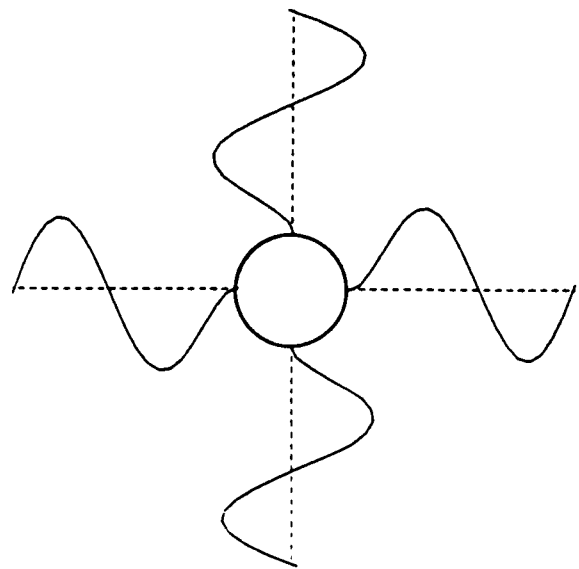depend on dt_f, the change in final time.

Figure 3-3. Model Structure

MODE 1, 1.261 Hz

MODE 2, 8.396 Hz   MODE 3, 24.905 Hz

Figure 3-4. Elastic Deflection Modes

As a result of many numerical simulations, it has been found that without modifications, the optimal perturbation feedback control, as presented in this chapter, performs poorly, especially towards the final time when the gains are large and vary quickly. One source of difficulty is due to the singularity of $\bar{Q}$. Since $\bar{Q}$ is singular, all of the feedback gains become infinite at the final time. Because of numerical inaccuracies, this results in randomly large gains near the final time. A remedy is to use $Q = -\varepsilon_1 I$, where ε_1 is a small positive number. The negative sign for Q is due to the fact that if Q were to be a function of time, it can be shown that $Q < 0$ for $t < t_f$. With this modification, the gains become large in a well-behaved manner near the final time.

Another difficulty manifests itself in the numerical instability of the final time estimation. Since the correction variable, ε, of (3.5.8) is computed as the difference of potentially large numbers (relative to ε), the calculation is easily numerically unstable when the values of $\hat{m}(t_I)$ and $\hat{n}(t_I)$ are large or corrupted by numerical inaccuracy. This results in values of ε alternating in sign and increasing in magnitude at each successive iteration, leading to an unstable algorithm. A remedy for this problem is to increase the magnitude of α in the expression following (3.4.2), using

$$\alpha = (1 + \varepsilon_2) \left[\frac{d\Omega}{dt}\right]\bigg|_{t_f} , \qquad (3.6.2)$$

where ε_2 is a small positive number. It is found that on choosing $\varepsilon_2 = 0.02$, the final time estimates become much better behaved, and the errors in satisfaction of the terminal constraints are reduced by about two or three orders of magnitude. If we use $\varepsilon_2 = 0.5$, the terminal errors are reduced by almost four orders of magnitude. However, with $\varepsilon_2 = 0.5$ the free-final-time controller behaves as if it were a fixed-final-time controller. From these observations, it is clear that the performance of the controller is extremely sensitive to the value of α. It is not obvious, however, that α should be modified rather than any other variable. Nor is it obvious what the mechanism is for the improvement of system performance, since the modification of α affects all of the gain

variables. However, it is interesting to note that the modified variables, Q and α, are diagonal blocks of the matrix coefficient of (3.4.2). The remaining diagonal block, $S = S_f$, also greatly affects system performance, as discussed in [10]. For the results of this section, values chosen for ϵ_1 and ϵ_2 are 10^{-10} and 0.02, respectively.

Cases 1 and 2 represent retargeting maneuvers, where the final hub orientation, angular rate, angular acceleration, and third time derivative of the hub angle are required to match a moving target whose motion is presumably known. The nominal target motion is a linear fly-by (see Fig. 3-5), where the target travels in a straight line at constant velocity. The structure is assumed to rotate about the z axis, with the appendages moving in the x-y plane. The components of the ψ vector are given in the following equations:

$$\theta(t_f) - \theta_T(t_f) = 0, \quad \theta_T(t_f) = \tan^{-1}(\tfrac{y}{x}) ,$$

$$\dot{\theta}(t_f) - \dot{\theta}_T(t_f) = 0, \quad \dot{\theta}_T(t_f) = \frac{vx}{x^2 + y^2} ,$$

$$\ddot{\theta}(t_f) - \ddot{\theta}_T(t_f) = 0, \quad \ddot{\theta}_T(t_f) = \frac{-2v^2 xy}{(x^2 + y^2)^2} ,$$

and

$$\dddot{\theta}(t_f) - \dddot{\theta}_T(t_f) = 0, \quad \dddot{\theta}_T(t_f) = \frac{8v^3 xy^2}{(x^2 + y^2)^3} - \frac{2v^3 x}{(x^2 + y^2)^2} ,$$

$$(3.6.4)$$

where $x = x_0$ and $y = y_0 + vt_f$. The perturbed target motion is also a constant-velocity linear fly-by, but with a different starting location and different velocity. The target parameters and weighting matrices are shown in Table 3-1. The weight on the elapsed time is adjusted so that the nominal final time is 5.0 s, for convenience. The terminal state weighting is computed using a modified version of the algorithm in [10]. Because of the large terminal weights on η_1 and $\dot{\eta}_1$, the final values of the remaining state variables are more or less constrained via the terminal constraint conditions of (3.6.3). Therefore, the elements in the
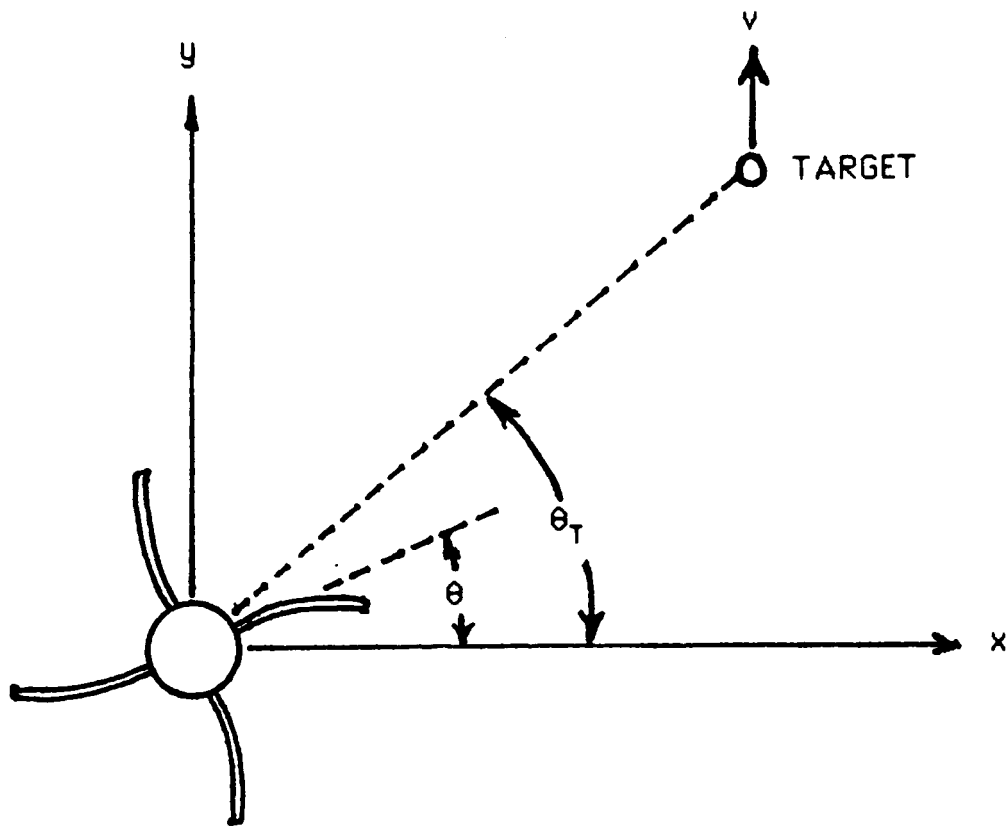
Figure 3-5. Linear Fly-By for Cases 1 and 2

Table 3-1. Maneuver Specifications for Cases 1 and 2

Weights

$$
S_f = \begin{bmatrix}
2.63(3) & & & & & \text{Symmetric} \\
3.95(3) & 3.09(6) & & & & \\
7.90 & -7.31(2) & 2.63(3) & & & \\
1.18(1) & 4.12(4) & 3.95(3) & 2.68(5) & & \\
6.24(-3) & -3.38(1) & 4.16 & 1.98(2) & 1.00(5) & \\
4.73(-6) & -3.52(-2) & 4.23(-3) & 2.01(-1) & 1.55(2) & 3.23(3)
\end{bmatrix}
$$

W_{xx} = Block diagonal $[W_{11}, W_{22}, 1.00(-5), 1.00(-5)]$

$$
W_{11} = \begin{bmatrix} 2.63(-5) & 3.95(-5) \\ 3.95(-5) & 6.91(-5) \end{bmatrix}
\qquad
W_{22} = \begin{bmatrix} 2.63(-5) & 3.95(-5) \\ 3.95(-5) & 6.91(-5) \end{bmatrix}
$$

$W_{uu} = [10]$

Nominal conditions:

$\theta(t_o) = \dot{\theta}(t_o) = \eta_1(t_o) = \dot{\eta}_1(t_o) = u(t_o) = \dot{u}(t_o) = 0$

$x_o = 2.7(7), \quad y_o = -4.0(4), \quad v = 8.0(3)$

Perturbed Conditions:

$\theta(t_o) = 2(-5)\text{rad}, \quad \dot{\theta}(t_o) = -2(-5) \text{ rad/s}$

$\eta_1(t_o) = \dot{\eta}_1(t_o) = u(t_o) = \dot{u}(t_o) = 0$

$x_o = 2.5(7), \quad y_o = -4.1(4), \quad v = 7.8(3)$

$a(n)$ indicates $a \times 10^n$

rows and columns of S_f corresponding to η_0, $\dot{\eta}_0$, u, and $\dot{u}$ can be set to very small numbers. However, because of numerical considerations, these elements are set to larger numbers to decrease the condition number of the $Z(t)$ matrix. The perturbed trajectory information for Case 2 is introduced into the feedback law at $t = 2.5$ s. This simulates the case when target information is updated during a maneuver.

The time history plots for Cases 1 and 2 are shown in Figures 3-6 through 3-8. For Case 1, note that all the terminal constraints are satisfied for both the nominal and perturbed trajectories. (The target angular acceleration, $\ddot{\theta}_T$, and third angular rate, $\dddot{\theta}_T$, are virtually zero at the final time for both the nominal and perturbed targets.) For Case 2, the hub angular acceleration shows a small terminal error. However, all other states reach their desired terminal values, including the control and its first derivative. The second derivative of the control torque shows a very small spike near the final time in Figure 3-8. Such spikes are typical when the final gains are large, and may be removed by appropriately adjusting S_f, Q, or α of (3.4.2).

3.7   Extensions

The closed-form solutions given in this paper are only applicable for control problems where the plant dynamics is linear time-invariant. For nonlinear systems, closed-form solutions are much more difficult to obtain. Nevertheless, one may use the following method with the closed-form solutions of this section to approximate the solution of the feedback gains for a nonlinear system. First, one obtains the nominal state and control time-histories, using numerical techniques such as shooting methods [23,30] and boundary-value continuation (see Sections 4.3.1 and 4.3.5). Second, the state differential equations are linearized about the nominal solution at discrete points in time. Third, piecewise linear time-invariant intervals are defined about these discrete points in time. Fourth, assuming that the feedback gains are continuous at the boundaries of these intervals, one can transfer the terminal conditions for $\hat{S}(t)$, $\hat{R}(t)$, $\hat{m}(t)$, and $\hat{n}(t)$ into initial conditions by sequentially computing the boundary conditions at each of the interval boundaries, using the
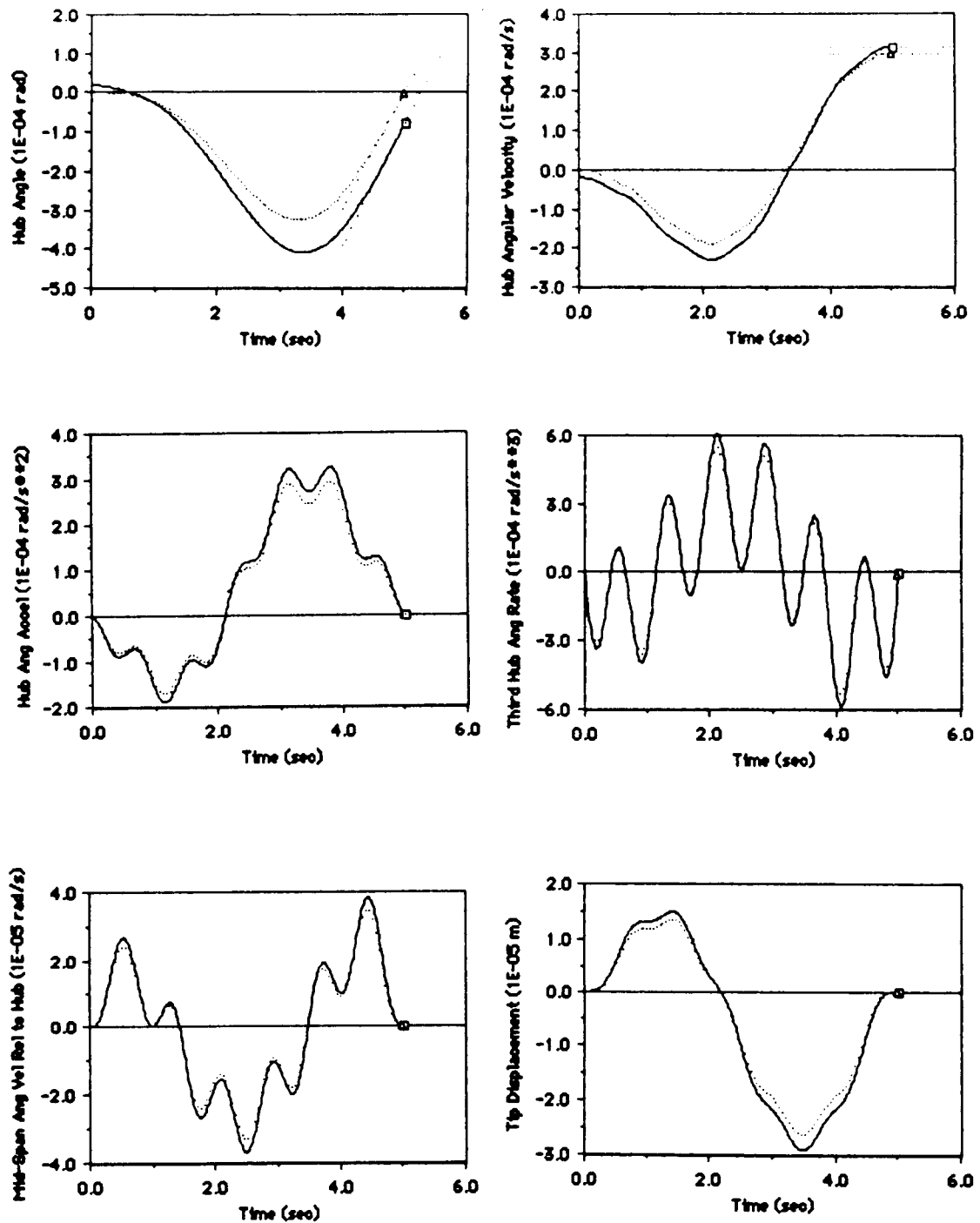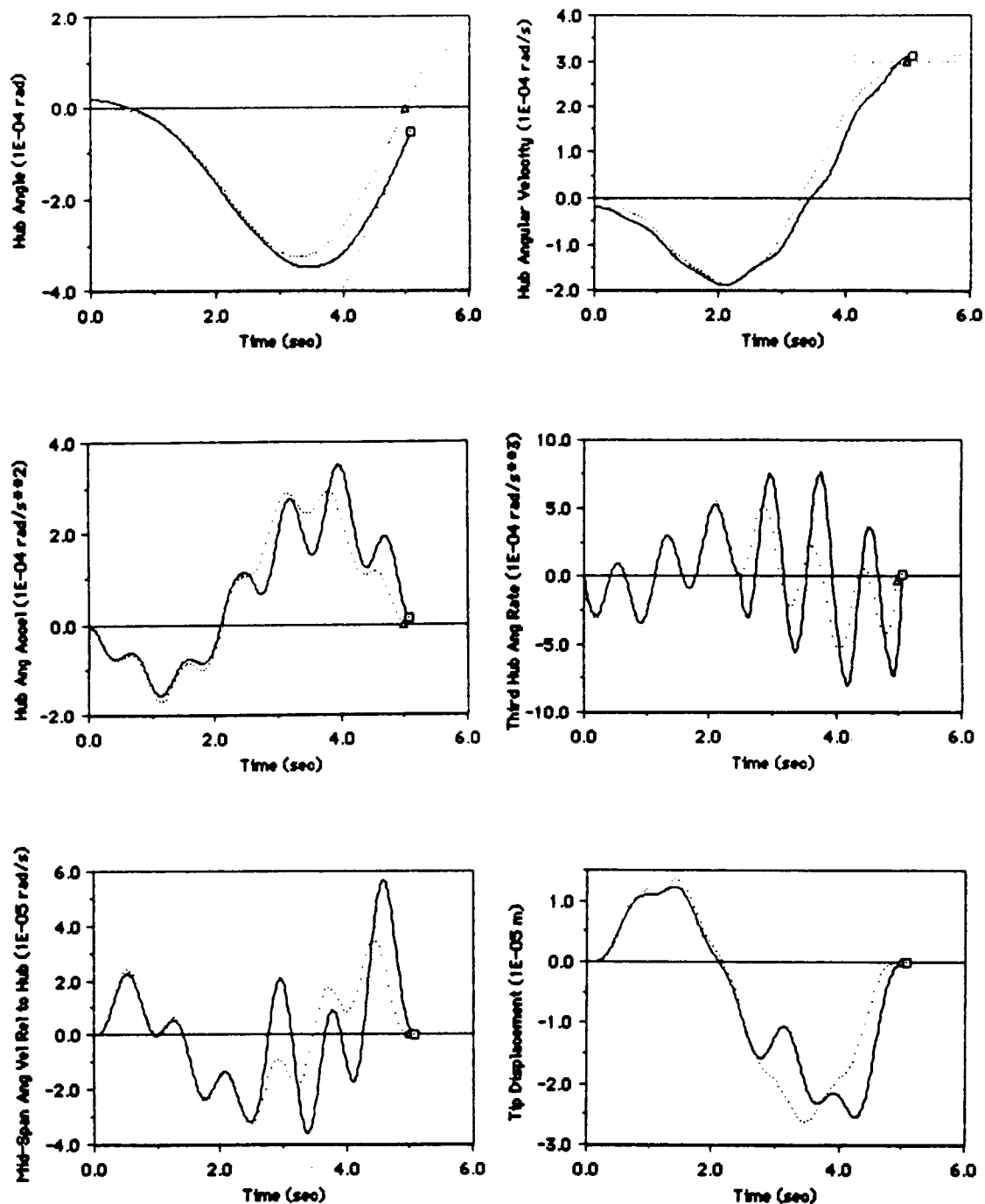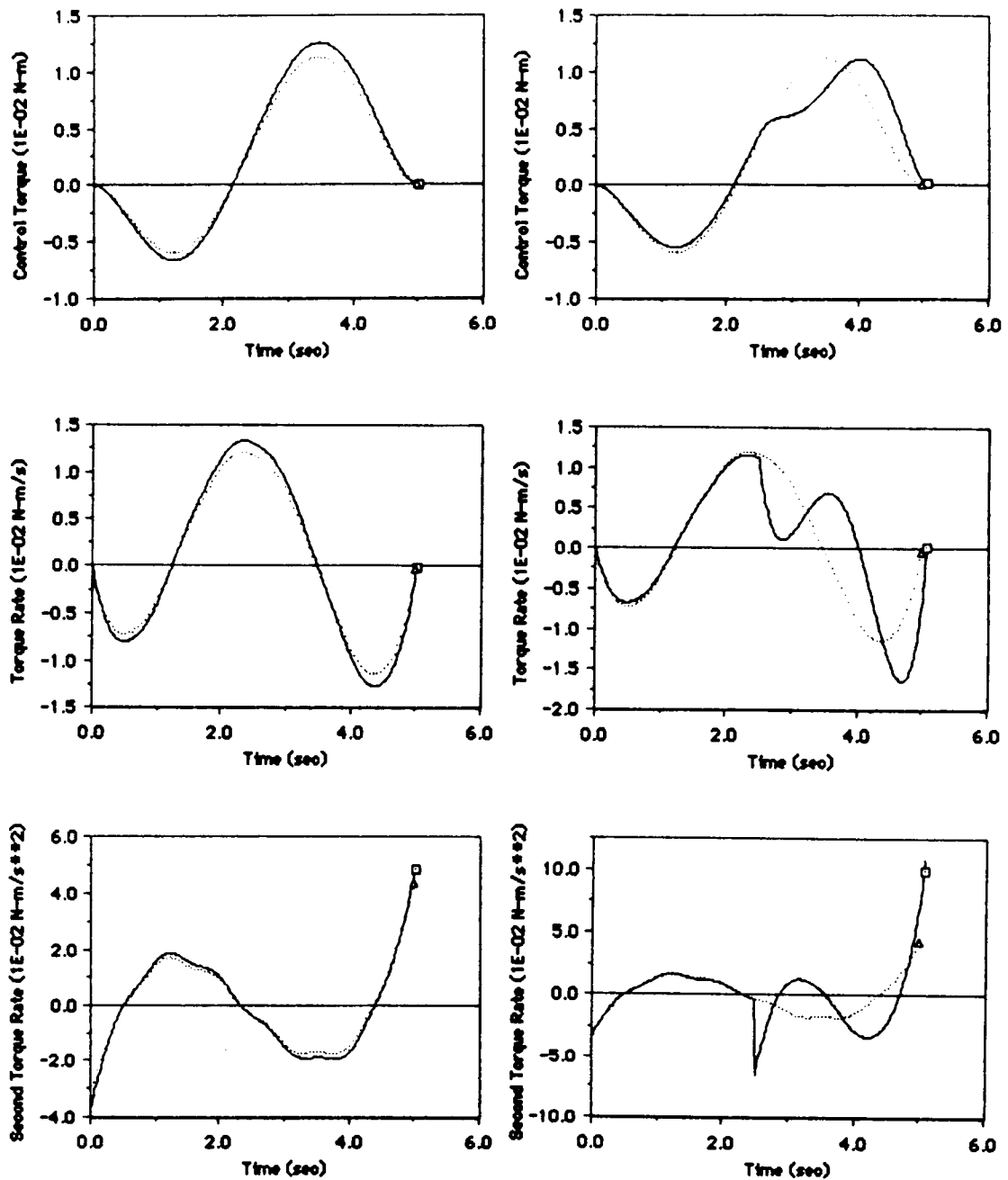
Figure 3-6. Case 1. Retargeting Maneuver

Figure 3-7.   Case 2.   Retargeting Maneuver with Changing
Terminal Constraints

a) Case 1   b) Case 2

Figure 3-8.   Control Trajectories for Cases 1 and 2

closed-form solutions, starting from the interval nearest the final time and going backwards in time. Finally, one can use the initial conditions for $\hat{S}(t)$, $\hat{R}(t)$, $\hat{m}(t)$, and $\hat{n}(t)$, with closed-form solutions and piece-wise linear time-invariant system differential equations to apply the feedback gains to the perturbed states and perturbed terminal constraints. The length of the linear time-invariant intervals may need to be adjusted depending on the degree of nonlinearity present at a given time along the nominal trajectory.

SECTION 4

NONLINEAR THREE-AXIS MANEUVERS FOR FLEXIBLE SPACECRAFT
WITH CONTROL SMOOTHING

4.1   Introduction

This section presents formulations for general nonlinear three-axis slewing maneuvers for flexible spacecraft. The approach used here is to find the optimal solution for the rigid body model, and then to apply this open-loop rigid body optimal control to the fully flexible spacecraft with a perturbation feedback controller. The perturbation feedback controller controls several flexible modes in addition to the rigid body modes, and the feedback gains are computed using the flexible plant linearized about the rigid body nominal solution at several points along the maneuver. An extended Kalman filter is implemented to estimate the plant states. Example maneuvers are shown using the model of a generic space vehicle.

Section 4.2 presents a discussion of model development and simulation issues. Section 4.3 presents the solution to the nonlinear rigid body problem. The flexible body perturbation formulation is developed in Section 4.4, and the extended Kalman filter is discussed in Section 4.5.

4.2   Model Development

The spacecraft model used for the example maneuvers of this section is based on a satellite model similar to the N-ROSS satellite, which consists of a more or less rigid bus and several flexible appendages (Figure 4-1). For this study, the spacecraft bus is assumed to be rigid, and only two of the appendages, namely the radiometer and the solar array, are assumed to be flexible. The frequencies and mode shapes of the flexible appendages are in the form of NASTRAN output data.
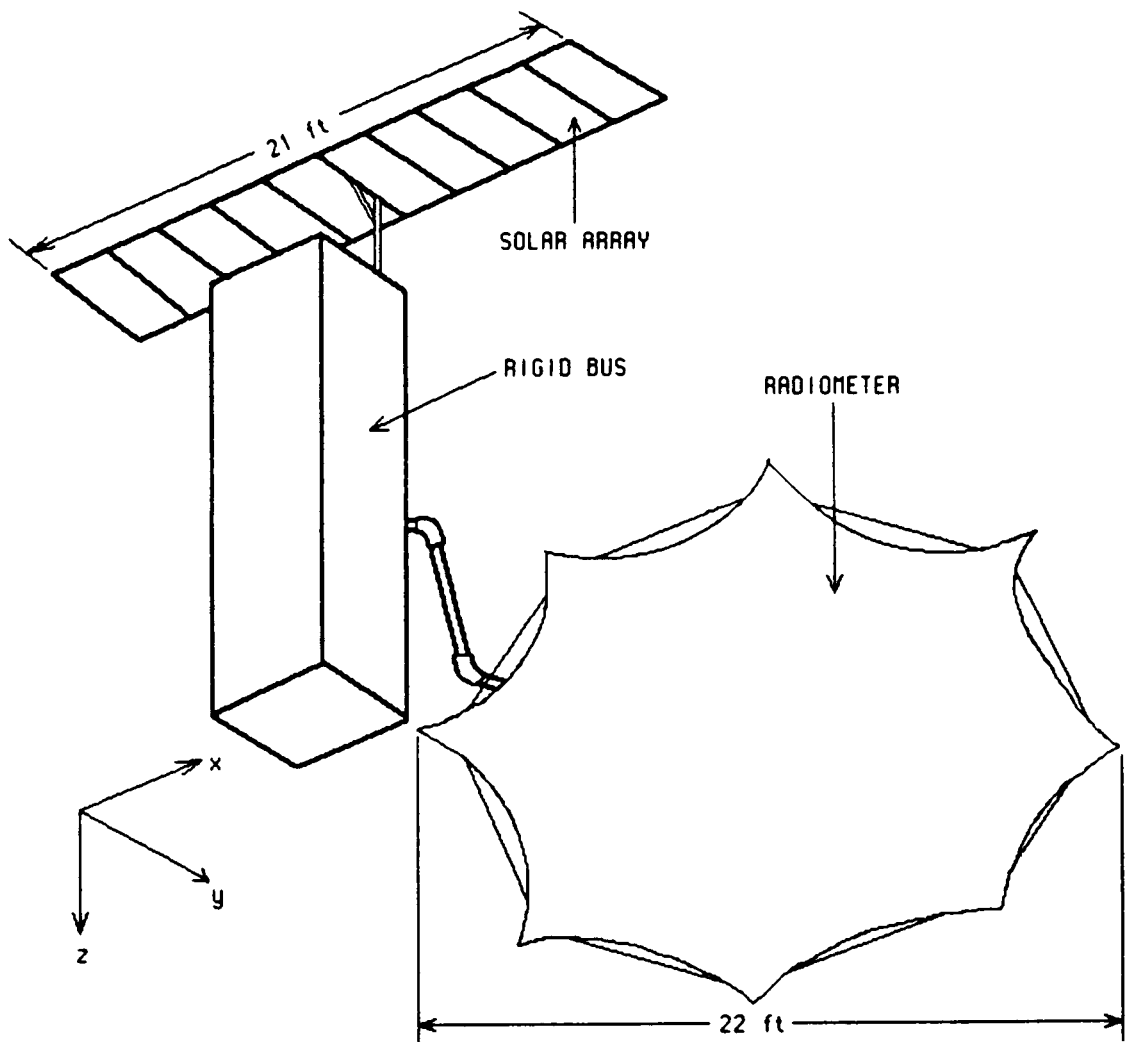
Figure 4-1. Spacecraft Model

The original spacecraft design has one rigid body and six flexible appendages. Since only two of the appendages are considered flexible for this study, the remaining appendages and the rigid body are lumped together to form one rigid body. The total system inertia matrix about the system center of mass is given in units of slug-ft^2 by

$$[I] = \begin{bmatrix} 3888 & -468.7 & 590.7 \\ -468.7 & 4242 & 570.2 \\ 590.7 & 570.2 & 2105 \end{bmatrix} . \qquad (4.2.1)$$

The flexible appendages are each assumed to have five elastic degrees of freedom, and their frequencies are listed in Table 4-1. Every mode is assumed to have 0.1% damping.

4.2.1 Multibody Dynamics Simulation

The numerical simulation for the example maneuvers was carried out using a program called DISCOS (Dynamic Interaction Simulation of Controls and Structures) [4], which is a well-known package of software developed for the National Aeronautics and Space Administration (NASA) and distributed by Computer Software Management and Information Center (COSMIC). In DISCOS, a complex structure may be modeled as several rigid or flexible structures connected together at specific points, called hinges. The equations of motion for each body may then be written in the same general form for a single body, with the coupling between bodies provided by Lagrange multipliers which maintain the desired interface constraints.

4.2.2 Recent Issues in Multibody Dynamics Simulation

Doubts have recently been cast on the validity of multibody computer programs such as DISCOS [4], NBOD [12], ALLFLEX [15,16] and TREETOPS [32]. Since DISCOS was chosen to simulate the three-dimensional nonlinear slews of this section, an investigation was carried out to determine the validity of such claims [19].

One of the claims was that current multibody computer programs do not include rotational inertia terms for the individual elements of a finite element model. However, as shown in Reference 9, by computing the inertia matrix for a single body from first principles, and comparing the result with the documentation for DISCOS [4], it is found that DISCOS does include rotational inertia terms for the individual elements of a finite-element model.

Another issue of concern is the absence of a gyroscopic stiffening/ arc length correction term in current multibody computer programs. The arc length correction involves the difference in distance to a point on a long slender beam when measured along the deformed beam and when measured as the projection onto the beam's undeformed position. Inclusion of this correction term leads to a stiffening term in the equations of motion, which increases with higher angular velocities, hence the term gyroscopic stiffening. Since this effect is applicable only to long slender rods, and is important only for high angular velocities, it is often not included in general multibody computer programs. For the example cases of this study, the angular velocites are small, hence the neglected gyroscopic stiffening/arc length correction terms are not important.

4.3   Optimal Nonlinear Three-Dimensional Maneuvers with Control Smoothing for Rigid Structures

This subsection deals with the solution for the open-loop nominal control profile which is based on a rigid body model. The solution to the nonlinear optimal control problem is obtained by first solving the problem of a single-axis maneuver with a diagonal inertia matrix, and then using a continuation method to introduce the three-axis boundary conditions and off-diagonal elements of the inertia matrix.

4.3.1 Continuation Method

The continuation method [29], also known as homotopy chain method, is a process by which a continuation parameter, α, is imbedded into the equations of a problem so that when α is set to zero, the modified problem becomes easy to solve, and when α is set to one, the modified problem reverts to the original hard-to-solve problem. Typically, the continuation parameter is used to multiply terms which make the problem difficult to solve.

There are many ways of sweeping the value of the continuation parameter from zero to one. One way is by numerical integration which requires the calculation of the derivative of the solution with respect to the continuation. For some problems, is is difficult to compute this derivative. Instead, a prediction-correction type of integration may be performed, where previously converged intermediate solutions are used to estimate the required derivative by means of finite differences. A more crude but simple approach is to slowly increment the value of α, and perform an iterative correction at each increment. This approach is less efficient, but involves the least amount of programming.

4.3.2 Equations of Motion

For the rigid body control problem, let us select as state variables Euler parameters, β, body angular velocities, ω, pseudo-controls, u_o, and pseudo-control rates, u_1. The pseudo-control vector is defined as

$$u_o = [I]^{-1} \left\{ \begin{array}{c} u_x \\ u_y \\ u_z \end{array} \right\} ,$$
(4.3.1)

where

$$[I] = \begin{bmatrix} I_{xx} & -I_{xy} & -I_{xz} \\ -I_{yx} & I_{yy} & -I_{yz} \\ -I_{zx} & -I_{zy} & I_{zz} \end{bmatrix} ,$$

and u_x, u_y, and u_z are torques about the x, y, and z axes, respectively. The torques are assumed to be applied by concentrated torque generating devices acting on the rigid spacecraft bus. The inclusion of the pseudo-controls and pseudo-control rates is for control smoothing, as described in Reference 9. Pseudo-controls are used instead of the actual applied torques because the use of applied torques results in large values for the angular velocity costates when the moments of inertia are large. By using pseudo-controls, the problem is normalized so that the values of the states and costates are close to the same order of magnitude. The equations of motion can be shown to be

$$\dot{\beta} = \Omega(\omega)\beta , \qquad\qquad (4 \times 1) \qquad (4.3.2)$$

$$\dot{\omega} = u_0 + G(\omega) , \qquad\qquad (3 \times 1) \qquad (4.3.3)$$

$$\dot{u}_0 = u_1 , \qquad\qquad (3 \times 1) \qquad (4.3.4)$$

and

$$\dot{u}_1 = u_2 , \qquad\qquad (3 \times 1) \qquad (4.3.5)$$

where

$$\Omega(\omega) \;\; = \;\; \frac{1}{2} \begin{bmatrix} 0 & -\omega_x & -\omega_y & -\omega_z \\ \omega_x & 0 & \omega_z & -\omega_y \\ \omega_y & -\omega_z & 0 & \omega_x \\ \omega_z & \omega_y & -\omega_x & 0 \end{bmatrix} \;\; ,$$

$$G(\omega) \;\; = \;\; - [I]^{-1} [\tilde{\omega}][I]\omega \;\; ,$$

$$\omega \;\; = \;\; [\omega_x \; \omega_y \; \omega_z]^T \;\; ,$$

and

$$[\tilde{\omega}] \;\; = \;\; \begin{bmatrix} 0 & -\omega_z & \omega_y \\ \omega_z & 0 & -\omega_x \\ -\omega_y & \omega_x & 0 \end{bmatrix} \;\; .$$

In the above equations, (4.3.2) is the kinematic equation relating the Euler parameter rates and the body angular velocities, and (4.3.3) represents Euler's equation in terms of pseudo-controls.

4.3.3 Optimal Control Problem and Necessary Conditions

For rigid body nonlinear three-dimensional slews, let us define the optimal control problem as the minimization of a finite-time quadratic performance index

$$J \;\; = \;\; \frac{1}{2} \int_{t_o}^{t_f} [\chi^T(t) \; u_2^T(t)] \; W \left\{ \begin{array}{c} \chi(t) \\ u_2(t) \end{array} \right\} \; dt \;\; , \tag{4.3.6}$$

where

$$\chi \;\; = \;\; [\beta^T \; \omega^T \; u_o^T \; u_1^T]^T \;\; ,$$

and

$$
W \;=\; \begin{bmatrix} 0 & 0 & 0 & 0 & 0 \\ 0 & Q & 0 & 0 & 0 \\ 0 & 0 & I & 0 & I/\omega_B^2 \\ 0 & 0 & 0 & 0 & 0 \\ 0 & 0 & I/\omega_B^2 & 0 & I/\omega_B^4 \end{bmatrix} ,
$$

subject to the state dynamics equations, (4.3.2) through (4.3.5), with specified initial and final states. The symbol I represents the (3 × 3) identity matrix. In the performance index of (4.3.6), the weight matrix, W, does not include penalties on the Euler parameters, since the angular displacements may be large. A weighting matrix is placed on the angular velocity terms so that the angular velocities may be kept small. The penalty terms on the pseudo-controls and pseudo-control rates are the time-domain equivalent of frequency-domain penalties on the pseudo-control, where the frequency range above ω_B is penalized (see Ref. 9).

The Hamiltonian for the performance index of (4.3.6) and the state dynamics of (4.3.2) through (4.3.5) may be written as

$$
H \;=\; \tfrac{1}{2}\big[\omega^T Q \omega + u_o^T u_o + u_2^T u_2/\omega_B^4 + 2 u_o^T u_2/\omega_B^2 \big]
$$

$$
+ \; \gamma^T \Omega(\omega)\beta + \lambda^T\big(u_o + G(\omega)\big) + \mu_o^T u_1 + \mu_1^T u_2 , \tag{4.3.7}
$$

where γ (4 × 1), λ (3 × 1), μ_o (3 × 1), and μ_1 (3 × 1) are costate or adjoint variables for β, ω, u_o, and u_1, respectively. The necessary conditions can then be derived from the Hamiltonian as

$$\left[\frac{\partial H}{\partial \gamma}\right]^T = \dot{\beta} = \Omega(\omega)\beta \ , \tag{4.3.8}$$

$$\left[\frac{\partial H}{\partial \lambda}\right]^T = \dot{\omega} = u_o + G(\omega) \ , \tag{4.3.9}$$

$$\left[\frac{\partial H}{\partial \mu_o}\right]^T = \dot{u}_o = u_1 \ , \tag{4.3.10}$$

$$\left[\frac{\partial H}{\partial \mu_1}\right]^T = \dot{u}_1 = u_2 \ , \tag{4.3.11}$$

$$- \left[\frac{\partial H}{\partial \beta}\right]^T = \dot{\gamma} = \Omega(\omega)\gamma \ , \tag{4.3.12}$$

$$- \left[\frac{\partial H}{\partial \omega}\right]^T = \dot{\lambda} = - Q\omega - \left[\frac{\partial}{\partial \omega}(\gamma^T \Omega \beta)\right]^T - \left[\frac{\partial G}{\partial \omega}\right]^T \lambda \ , \tag{4.3.13}$$

$$- \left[\frac{\partial H}{\partial u_o}\right]^T = \dot{\mu}_o = - u_o - u_2/\omega_B^2 - \lambda \ , \tag{4.3.14}$$

$$- \left[\frac{\partial H}{\partial u_1}\right]^T = \dot{\mu}_1 = - \mu_o \ , \tag{4.3.15}$$

and

$$\left[\frac{\partial H}{\partial u_2}\right]^T = 0 = u_2/\omega_B^4 + u_o/\omega_B^2 + \mu_1 \ , \tag{4.3.16}$$

where the following notation has been used

$$\left[\frac{\partial v}{\partial w}\right]_{ij} = \frac{\partial v_i}{\partial w_j} \ ,$$

for general vectors (or scalars) v and w. In the equations above, the initial and final values for β, ω, u_o and u_1 are specified. However, no boundary conditions are known for γ, λ, μ_o, and μ_1.

4.3.4 Starting Guess for the Continuation Method

The necessary conditions for the rigid body slewing problem shown in (4.3.8) through (4.3.16) represent a set of difficult nonlinear differential equations with split boundary conditions. To solve the differential equations, a continuation method is used, as discussed in Section 4.3.1. The first step is to find a starting guess which is easy to solve. For this, we choose a single-axis maneuver about a principle axis. To further simplify the calculations, we assume initially that the inertia matrix of the spacecraft is diagonal, with the non-zero off-diagonal terms introduced during the continuation process.

A reasonable choice of axis for the starting guess solution is to use the axis with the highest peak angular momentum if the single-axis maneuver were to be accomplished via bang-bang control. This is also the axis about which the largest bang-bang torque would be applied. Denoting this axis by k, where k = 1, 2, or 3 corresponds to the x, y, or z axis, one may write a modified subset of the necessary conditions of (4.3.8) through (4.3.16) for rotation about axis k:

$$\dot{\chi}(t) = [K]\chi(t), \qquad\qquad (4.3.17)$$

where

$$\chi(t) = \left\{ \begin{array}{c} \phi_k(t) - \phi_k(t_o) \\[6pt] \omega_k(t) \\[6pt] [u_o(t)]_k \\[6pt] [u_1(t)]_k \\[6pt] [\mu_o(t)]_k \\[6pt] [\mu_1(t)]_k \\[6pt] \xi(t) \\[6pt] c \end{array} \right\}$$

$$[K] = \begin{bmatrix} 0 & 1 & 0 & 0 & 0 & 0 & 0 & 0 \\ 0 & 0 & 1 & 0 & 0 & 0 & 0 & 0 \\ 0 & 0 & 0 & 1 & 0 & 0 & 0 & 0 \\ 0 & 0 & -\omega_B^2 & 0 & 0 & -\omega_B^4 & 0 & 0 \\ Q_k & 0 & 0 & 0 & 0 & \omega_B^2 & -1 & 0 \\ 0 & 0 & 0 & 0 & -1 & 0 & 0 & 0 \\ 0 & 0 & 0 & 0 & 0 & 0 & 0 & -\frac{1}{2} \\ 0 & 0 & 0 & 0 & 0 & 0 & 0 & 0 \end{bmatrix} \quad ,$$

$$\xi(t) = \lambda_k(t_o) - \frac{1}{2}(t-t_o)\,C,$$

$$C = \gamma_k(t_o)\sec\{\phi_k(t_o)/2\} \quad ,$$

and $\phi_k(t)$ is the angular displacement about axis k. In deriving (4.3.17), we have imposed the orthogonality constraint:

$$\sum_{i=1}^{4} \beta_i \gamma_i = 0 \qquad\qquad (4.3.18)$$

to ensure uniqueness of the Euler parameter costates.

Since (4.3.17) represents a linear time-invariant system, the final values of $\chi(t)$ can be related to the initial values by an equation of the form

$$\chi(t_f) = e^{K(t_f-t_o)}\chi(t_o) \quad . \qquad\qquad (4.3.19)$$

Observing that the initial and final values for ϕ_k, ω_k, $(u_o)_k$, and $(u_1)_k$ are known, one can perform the partitioned matrix multiplication in (4.3.19) for the upper partition of $\chi(t_f)$, and solve for the unknown initial values of $(\mu_o)_k$, $(\mu_1)_k$, ξ, and the unknown constant C, via

$$\Theta_{12} \begin{Bmatrix} (\mu_o)_k(t_o) \\ (\mu_1)_k(t_o) \\ \xi(t_o) \\ C \end{Bmatrix} = \begin{Bmatrix} \phi_k(t_f) - \phi_k(t_o) \\ \omega_k(t_f) \\ (u_o)_k(t_f) \\ (u_1)_k(t_f) \end{Bmatrix} - \Theta_{11} \begin{Bmatrix} 0 \\ \omega_k(t_o) \\ (u_o)_k(t_o) \\ (u_1)_k(t_f) \end{Bmatrix} ,$$

(4.3.20)

where

$$e^{K(t_f - t_o)} = \begin{bmatrix} \Theta_{11} & \Theta_{12} \\ \Theta_{21} & \Theta_{22} \end{bmatrix} .$$

The initial values of β_o, β_k, γ_o, γ_k, and λ_k are then given in terms of elements of $\chi(t_o)$ by

$$\beta_o(t_o) = \cos(\phi_k(t_o)/2) , \tag{4.3.21}$$

$$\beta_k(t_o) = \sin(\phi_k(t_o)/2) , \tag{4.3.22}$$

$$\gamma_o(t_o) = - C \sin(\phi_k(t_o)/2) , \tag{4.3.23}$$

$$\gamma_k(t_o) = C \cos(\phi_k(t_o)/2) , \tag{4.3.24}$$

and

$$\lambda_k(t_o) = \xi(t_o) . \tag{4.3.25}$$

The initial conditions of (4.3.21) through (4.3.25), together with $\omega_k(t_o)$, $[u_o(t_o)]_k$, $[u_1(t_o)]_k$, $[\mu_o(t_o)]_k$, and $[\mu_1(t_o)]_k$ of $\chi(t_o)$ comprise a complete set of initial conditions for a single-axis maneuver with a diagonal inertia matrix.

4.3.5 Continuation for Inertia Matrix and Boundary Conditions

Given the single-axis rotation with diagonal inertia matrix starting guess of Section 4.3.4, the three-axis optimal maneuver with fully populated inertia matrix may be obtained through a continuation process. The continuation approach used is one where the continuation parameter, α, is incremented at discrete steps, with convergence at each step achieved via a Newton-Raphson iteration.

Since there are two different quantities introduced during the continuation process--off-diagonal elements of the inertia matrix and three-axis boundary conditions--the continuation process may be performed separately or combined together in one process. When one combined continuation process is used, it may be advantageous to retain the ability to use separate continuation parameter increments for the two quantities when handling extremely difficult problems.

For the inertia matrix continuation, the inertia matrix of (4.3.1) is replaced by

$$
[I(\alpha_1)] = \begin{bmatrix} I_{xx} & -\alpha_1 I_{xy} & -\alpha_1 I_{xz} \\ -\alpha_1 I_{yx} & I_{yy} & -\alpha_1 I_{yz} \\ -\alpha_1 I_{zx} & -\alpha_1 I_{zy} & I_{zz} \end{bmatrix} .
\tag{4.3.26}
$$

Setting $\alpha_1 = 0$ produces the diagonal inertia matrix used in Section 4.3.4, and setting $\alpha_1 = 1$ produces the original fully populated inertia matrix.

For the boundary condition continuation, let us define the modified terminal Euler angles as

$$
\psi_j(t_f, \alpha_2) = \begin{cases} \phi_j(t_f) , & j = k \\ \alpha_2 \phi_j(t_f) , & j \neq k \end{cases}
\tag{4.3.27}
$$

where k represents the axis used for the starting guess of Section 4.3.4, and $\phi_j(t_f)$, (j=1,2,3), are the desired final Euler angles of the three-axis maneuver. For each value of the continuation parameter, α_2, the

modified final Euler parameters are computed from the values of ψ_j. The modified final conditions for the angular velocities, pseudo-controls, and pseudo-control rates are similarly defined as

$$\omega_j(t_f, \alpha_2) = \begin{cases} \omega_j(t_f) & j = k , \\ \alpha_2 \omega_j(t_f) & j \neq k , \end{cases} \qquad (4.3.28)$$

$$(u_o)_j(t_f, \alpha_2) = \begin{cases} (u_o)_j(t_f) & j = k , \\ \alpha_2(u_o)_j(t_f) & j \neq k , \end{cases} \qquad (4.3.29)$$

and

$$(u_1)_j(t_f, \alpha_2) = \begin{cases} (u_1)_j(t_f) & j = k , \\ \alpha_2(u_1)_j(t_f) & j \neq k . \end{cases} \qquad (4.3.30)$$

The modified initial conditions are defined in the same manner as for the modified final conditions.

After each increase of the continuation parameters, the previously converged values of the initial costates no longer generate trajectories which satisfy the final boundary conditions. As a result, an iterative correction scheme is needed to correct the initial costates based on the error in satisfying the final boundary conditions. For this purpose, a Newton-Raphson first-order correction scheme is used. This is accomplished by Taylor expanding the terminal values of the states as functions of the initial costates. As a result, the partial of the final states with respect to the initial costates must be computed. To obtain quicker convergence, one may use extrapolated values of the initial costates based on previously converged values and back α values [8,29,34].

For each iteration, the modified state-costate vector is integrated from t_o to t_f, and the error in satisfaction of the modified final conditions is computed. To obtain the partial of the final states with respect to the initial costates, one must integrate the partials of the state-costate vector with respect to the initial costates, along with the integration of the state-costate vector. That is, the matrices

$$\frac{\partial \chi(t)}{\partial \Lambda(t_o)} \qquad \text{and} \qquad \frac{\partial \Lambda(t)}{\partial \Lambda(t_o)}$$

are integrated from t_o to t_f, where

$$\Lambda = [\gamma^T \ \lambda^T \ \mu_o^T \ \mu_1^T]^T , \qquad\qquad (4.3.31)$$

and χ is defined following (4.3.6). The initial conditions and differential equations for integrating these partials are presented in Reference 9. The corrected costates for the next iteration are obtained as follows:

$$\Lambda_{I+1}(t_o,\alpha) = \Lambda_I(t_o,\alpha) - \bar{\Phi}^{-1}[\bar{\chi}_I(t_f,\alpha) - \bar{\chi}_d(t_f,\alpha)] , \qquad (4.3.32)$$

where

$$\alpha = [\alpha_1 \ \alpha_2]^T ,$$

$$\bar{\chi}_d(t_f,\alpha) = [0 \ \beta_1 \ \beta_2 \ \beta_3 \ \omega^T \ u_o^T \ u_1^T]_d^T \Big|_{t_f,\alpha} ,$$

$$\bar{\chi}_I(t_f,\alpha) = [0 \ \beta_1 \ \beta_2 \ \beta_3 \ \omega^T \ u_o^T \ u_1^T]_I^T \Big|_{t_f,\alpha} ,$$

$$\bar{\Phi} = \begin{bmatrix} \beta_0(t_o,\alpha) & \cdots & \beta_3(t_o,\alpha) & 0 & \cdots & 0 \\ \Phi_{\chi_2 \Lambda_1} & & \cdots & & & \Phi_{\chi_2 \Lambda_{13}} \\ \cdot & & & & & \cdot \\ \cdot & & & & & \cdot \\ \cdot & & & & & \cdot \\ \Phi_{\chi_{13} \Lambda_1} & & \cdots & & & \Phi_{\chi_{13} \Lambda_{13}} \end{bmatrix} ,$$

and

$$\Phi_{\chi_i \Lambda_j} = \frac{\partial \chi_i(t_f,\alpha)}{\partial \Lambda_j(t_o,\alpha)} \Big|_I .$$

In (4.3.2), the subscript d for $\chi_d(t_f,\alpha)$ indicates the desired modified final values, and the subscript I for $\bar{\chi}_I(t_f,\alpha)$ indicates the integrated final values for the current iterate. The variables $\bar{\chi}_d(t_f,\alpha)$, $\bar{\chi}_I(t_f,\alpha)$, and $\bar{\Phi}$ represent modified forms of $\chi_d(t_f,\alpha)$, $\chi_I(t_f,\alpha)$, and $\partial\chi(t_f,\alpha)/\partial\Lambda(t_o,\alpha)$, where the modification has been performed by replacing the first row of the Taylor expansion for $\chi(t_f,\alpha)$ by the orthogonality constraint [36]

$$\beta^T(t_o,\alpha)\gamma_d(t_o,\alpha) = 0 , \tag{4.3.33}$$

where $\gamma_d(t_o,\alpha)$ is the desired initial Euler parameter costate.

The entire continuation process is summarized in algorithmic form as follows. (The single-axis diagonal inertia matrix starting guess of Section 4.3.4 is assumed to have been computed.)

Step 1. If $\alpha_1 = 1$ and $\alpha_2 = 1$, stop. (end of continuation). Otherwise, increment α_1 and α_2, and compute $[I(\alpha_1)]$, $\chi(t_o,\alpha_2)$, and $\chi(t_f,\alpha_2)$.

Step 2. Integrate state-costate differential equations $((4.3.8)$ through $(4.3.15))$, and state-costate partials with respect to initial costates (Reference 9).

Step 3. Compute error in satisfaction of modified final boundary conditions. If small, go to Step 1.

Step 4. Compute new initial costates $((4.3.32))$. Go to Step 2.

4.3.6 Numerical Results

A 60 second rest-to-rest maneuver with angular displacements of 1 radian about each axis (using a 1-2-3 Euler sequence) is simulated. The weighting matrix for the angular velocity is arbitrarily chosen as $Q = 10^{-3}I$, where I is the (3 × 3) identity matrix. In choosing the value

for the break frequency, ω_B, it is found that it is best to choose ω_B so that it corresponds to the frequency of the maneuver; that is,

$$\omega_B = \frac{2\pi}{(t_f - t_o)} .$$

(4.3.34)

For the above value of ω_B, the resulting maneuver has pseudo-controls with smooth profiles (Figure 4-2). For higher values of ω_B, the pseudo-control profiles of the resulting maneuver have more undulations (see Figure 4-3). This reflects the higher frequency content of the controls, directly resulting from the higher value of ω_B. For lower values of ω_B, the resulting trajectories are similar to the case where ω_B is chosen according to (4.3.34). However, the number of Newton-Raphson iterations required for convergence is increased slightly, indicating that the partial derivative matrix of (4.3.32) may have become numerically stiffer. To illustrate the effect of the choice of ω_B on the frequency content of the resulting control, Figure 4-4 shows the frequency spectra of the pseudo-control for the single-axis starting guesses with ω_B corresponding to Figures 4-2, and 4-3. Because the penalty function of (4.3.6) penalizes the frequency content of the pseudo-controls for values of frequency above ω_B, one sees a sharp roll-off near ω_B in Figure 4-4.

4.4   Perturbation Feedback for Controlling the Flexible Body Response

4.4.1   Plant Linearization and Gain Calculation

This section presents a perturbation feedback scheme for controlling the elastic deformations of a flexible body when subjected to the nominal rigid body torque profile of Section 4.3. The flexible plant dynamics is linearized about the rigid body nominal solution at several points in time. Steady-state feedback gains are computed based on these linearized plants and an infinite-time performance index with control-rate penalty.

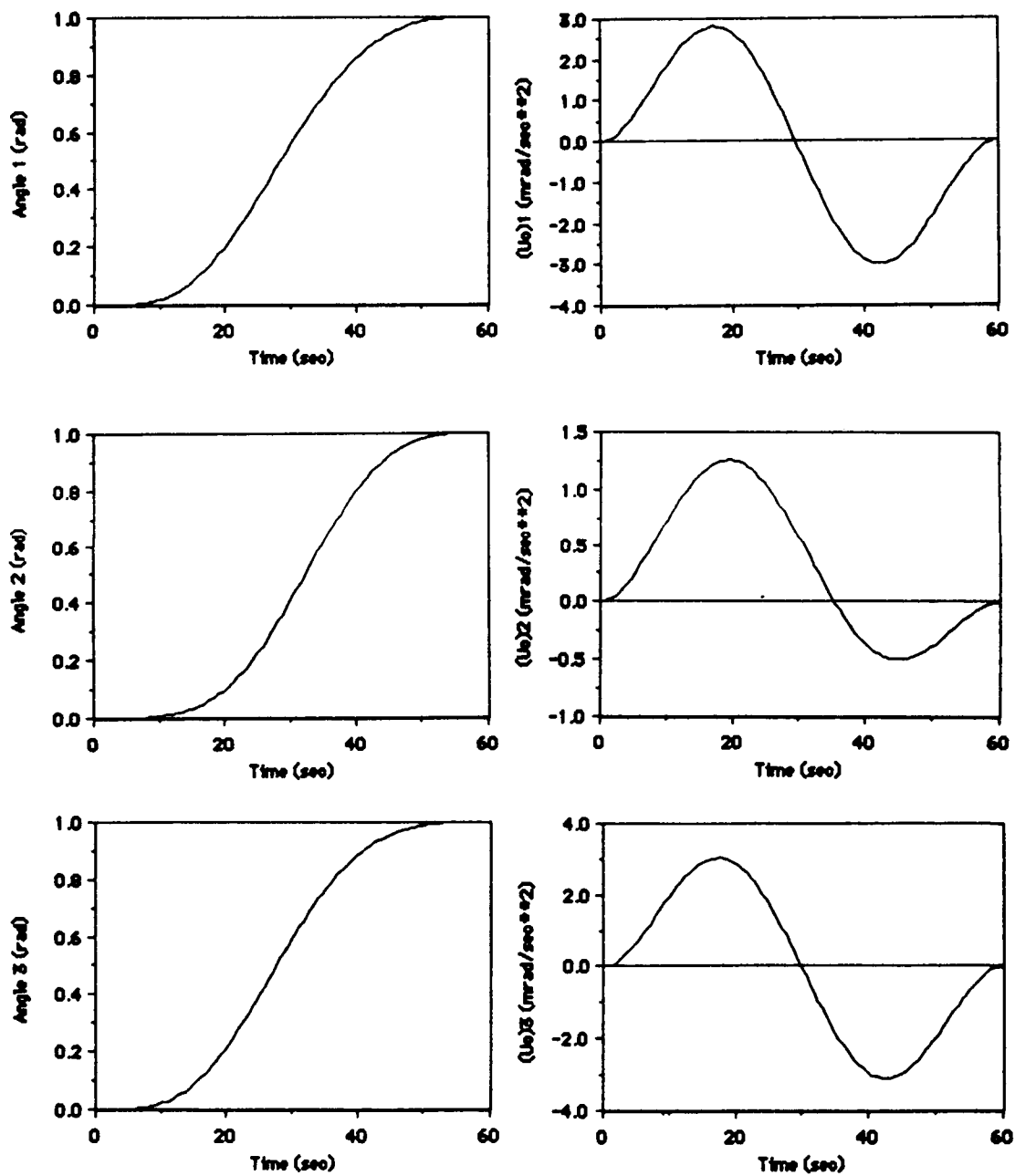The state perturbations used for the flexible plant model for the perturbation feedback are

Figure 4-2. Rigid Body Angle and Pseudo-Control
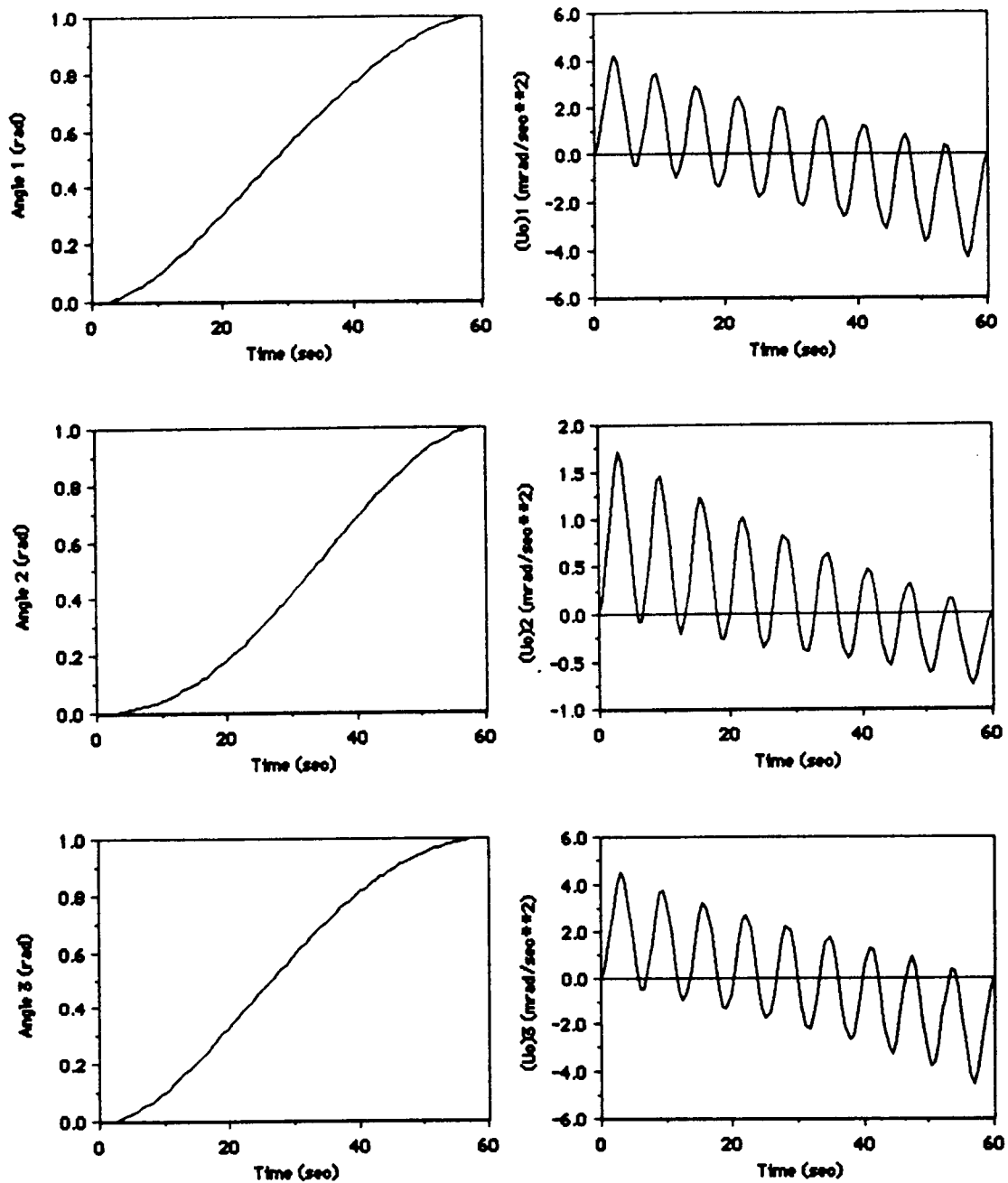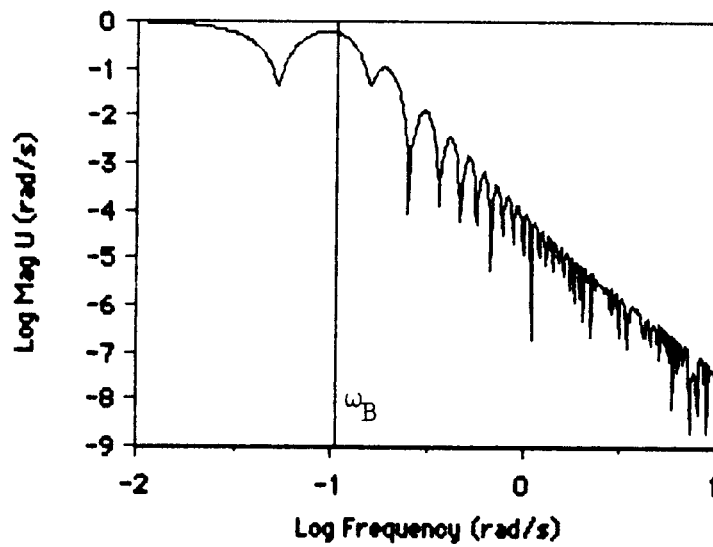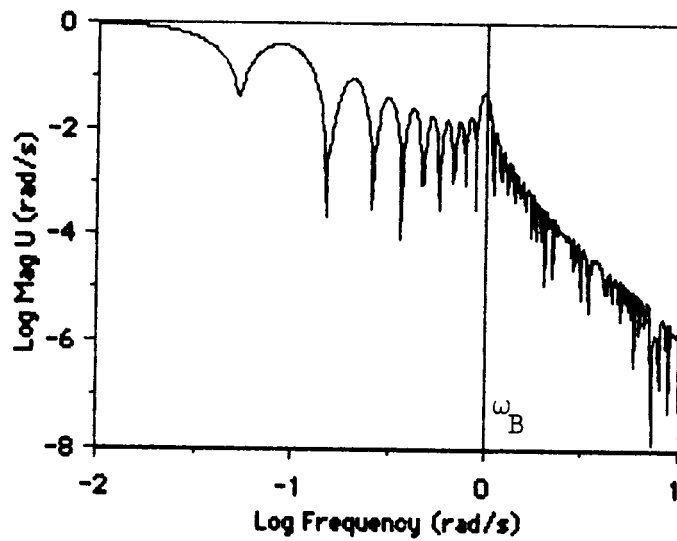Profiles for $\omega_B = 2\pi/60 = 0.1047$ rad/s

Figure 4-3.   Rigid Body Angle and Pseudo-Control Profiles
for ω_B = 1.0 rad/s

a) $\omega_B = 0.1047$ rad/s

b) $\omega_B = 1.0$ rad/s

Figure 4-4.   Frequency Spectra of the Pseudo-Controls for Starting
          Guesses with $\omega_B = 0.1047$ rad/s and $\omega_B = 1.0$ rad/s

$$\delta x = [\delta\omega_x \ \delta\omega_y \ \delta\omega_z \ \dot{\xi}_S^T \ \dot{\xi}_R^T \ \xi_S^T \ \xi_R^T \ \delta\phi_x \ \delta\phi_y \ \delta\phi_z]^T , \qquad (4.4.1)$$

where $\delta\omega_x$, $\delta\omega_y$, and $\delta\omega_z$ are the perturbed body angular velocities of the spacecraft bus, ξ_S and ξ_R are the modal amplitudes of the solar array and the radiometer, respectively, and $\delta\phi_x$, $\delta\phi_y$, and $\delta\phi_z$ are angular displacements of the spacecraft bus. The modal amplitudes, ξ_S and ξ_R, represent a reduced order elastic model. The numerical simulation includes several additional elastic modes to represent the residual mode responses.

From DISCOS, the linearized system dynamics and control influence matrices are obtained numerically through a quadratic finite difference approximation. The linearized differential equation for the state perturbations is then

$$\delta\dot{x}(t) = A^{(i)}\delta x(t) + B^{(i)}\delta u_o(t) , \qquad t = t_i , \qquad (4.4.2)$$

where t_i is the instant in time at which the plant is linearized, $A^{(i)}$ and $B^{(i)}$ are the linearized state dynamics and control influence matrices at $t = t_i$, and $u_o(t)$ is the pseudo-control.

For control-smoothing, the above differential equations are augmented by the differential equations for the perturbed pseudo-control:

$$\delta\dot{u}_o = \delta u_1 , \qquad (4.4.3)$$

and

$$\delta\dot{u}_1 = \delta u_2 . \qquad (4.4.4)$$

The performance index used for computing each set of steady-state gains is

$$J = \frac{1}{2} \int_{t_o}^{\infty} [\delta x^T(t) \; \delta u_o^T(t) \; \delta u_1^T(t) \; \delta u_2^T(t)] \; W \left\{ \begin{array}{c} \delta x(t) \\ \delta u_o(t) \\ \delta u_1(t) \\ \delta u_2(t) \end{array} \right\} dt \; , \qquad (4.4.5)$$

where

$$W = \begin{bmatrix} Q & 0 & 0 & 0 \\ 0 & I & 0 & I/\omega_B^2 \\ 0 & 0 & 0 & 0 \\ 0 & I/\omega_B^2 & 0 & I/\omega_B^4 \end{bmatrix} \; .$$

The penalties on the pseudo-controls, and their rates are in the form used in Gupta's frequency-shaped control smoothing where the break frequency, ω_B, may be different from the one used for the rigid body nominal. For each linearized plant, steady-state gains are computed based on the performance index of (4.4.5), and the dynamics equations of (4.4.2) through (4.4.4). Since the performance index is not rigorously minimized for the nonlinear plant, this feedback approach is suboptimal with respect to the performance index of (4.4.5).

For a given plant, described by $A^{(i)}$ and $B^{(i)}$, the optimal steady-state feedback solution for minimizing the performance index of (4.4.5) is given by

$$\delta u_2(t) = -R^{-1}[\tilde{B}^T P_{ss}^{(i)} + N^T] \delta \bar{\chi}(t) \; , \qquad (4.4.6)$$

where

$$R = I/\omega_B^4 \; , \qquad N^T = [0 \; \; I/\omega_B^2 \; \; 0] \; ,$$

$$\tilde{Q} = \begin{bmatrix} Q & 0 & 0 \\ 0 & I & 0 \\ 0 & 0 & 0 \end{bmatrix}, \qquad W = \begin{bmatrix} \tilde{Q} & N \\ N^T & R \end{bmatrix},$$

$$\tilde{A} = \begin{bmatrix} A^{(i)} & B^{(i)} & 0 \\ 0 & 0 & I \\ 0 & 0 & 0 \end{bmatrix}, \qquad \tilde{B}^T = [0 \quad 0 \quad I],$$

$$0 = P_{ss}^{(i)}\tilde{A} + \tilde{A}^T P_{ss}^{(i)} - [P_{ss}^{(i)}\tilde{B} + N]R^{-1}[N^T + \tilde{B}^T P_{ss}^{(i)}] + \tilde{Q},$$

and

$$\delta\bar{\chi}(t) = [\delta x^T(t) \quad \delta u_o^T(t) \quad \delta u_1^T(t)]^T.$$

During the perturbation feedback, the feedback gains are linearly interpolated between the points in time at which the gains are computed.

4.4.2 Numerical Results

Example cases are generated with the assumption of perfect state estimation. (Section 4.5 shows example cases where the Kalman filter is used for state estimation.) The 60 second rest-to-rest maneuver discussed in Section 4.3.6 is used for the nominal trajectory. The flexible plant is linearized about the rigid body nominal solution at 12 second intervals. Several off-nominal cases are studied. For all cases, the two lowest solar array modes and the two lowest radiometer modes are chosen for inclusion in the feedback formulation. The other higher frequency modes represent residual modes. All modes are assumed to have 0.1% damping. The break frequency for the perturbation controller, ω_B, is chosen to be half the frequency of the highest controlled mode, so as to minimize the excitation of the residual modes. Figure 4-5 shows the frequency spectra of the pseudo-control corrections when the perturbation feedback controller is subjected to initial conditions.

Log Mag u1 (rad/s)

Log Freq (rad/s)

Log Mag u2 (rad/s)

Log Freq (rad/s)

Log Mag u3 (rad/s)

Log Freq (rad/s)

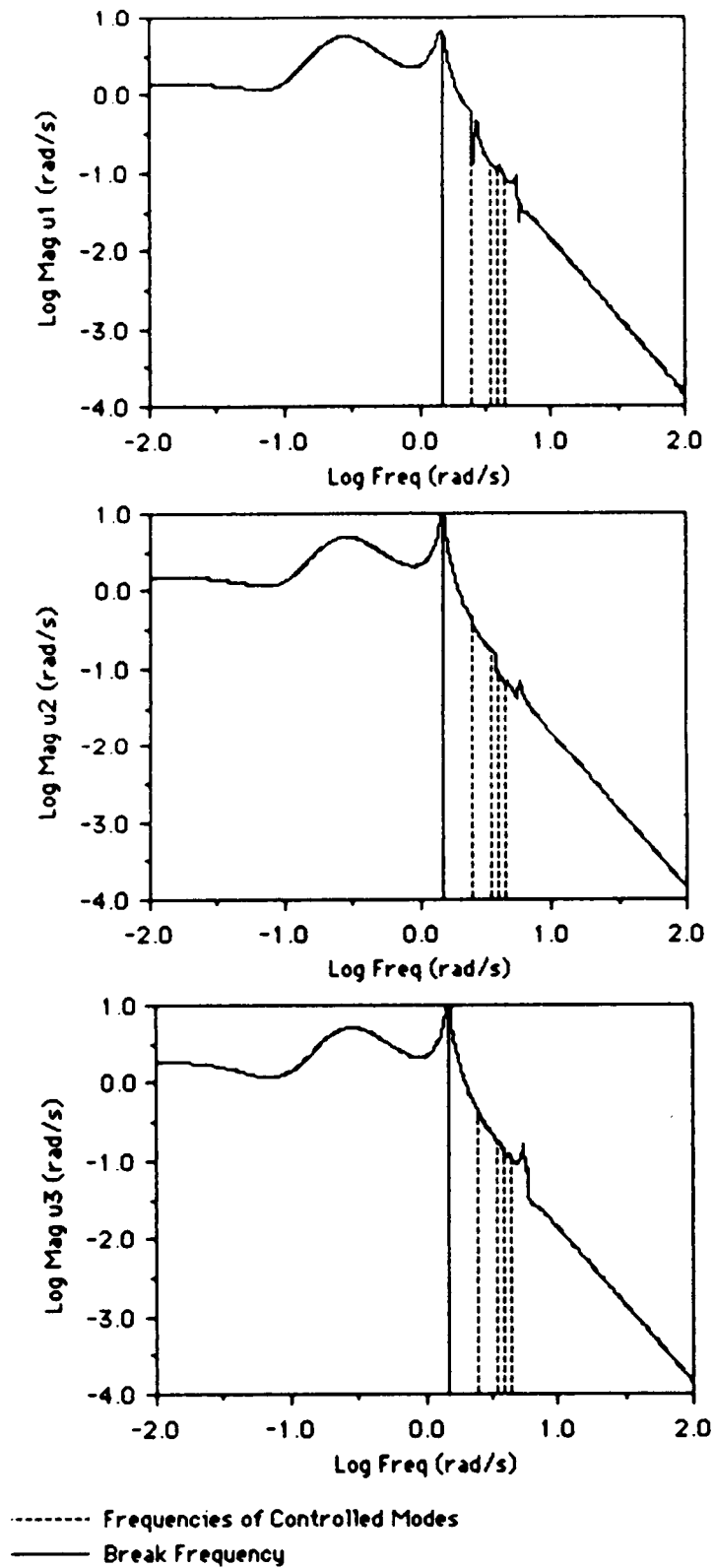-------- Frequencies of Controlled Modes

———— Break Frequency

Figure 4-5. Typical Frequency Spectra of the
Pseudo-Control Corrections

Case 1 (Figure 4-6) is the 'nominal' flexible body case, with perfect plant knowledge and nominal initial conditions. The controlled modal amplitudes and residual modal amplitudes for the solar array (denoted as S/A) and the radiometer are plotted separately. Note that all the modal amplitudes are very small by the end of the maneuver. The angle errors take a slightly longer time to settle. The pseudo-control corrections (denoted by Del u), take about 20 seconds beyond the maneuver time to damp out. For the case where the moments of inertia of the rigid bus are altered by 10%, the modal amplitude profiles are almost identical to those of Case 1, while the angle error histories and pseudo-control corrections are altered in amplitude.

Case 2 (Figures 4-7 and 4-8) is the same as Case 1, except that initial angular errors are specified for Case 2. The error in the initial angle is chosen to be 5% of the total angular displacement about each Euler axis. The sign of each of the errors is arbitrarily assigned. Note that the initial angular errors are an order of magnitude higher than the peak angular errors shown in Case 1. After about 20 seconds, the angular error and modal amplitude time histories approach the general shapes of the corresponding plots for Case 1. Since the peak values for the pseudo-control corrections are more than an order of magnitude higher than those for Case 1, the peak modal amplitudes are also higher than in Case 1. It appears that the oscillations in the pseudo-control corrections near the initial time may have excited the third radiometer mode (a residual mode). Additional example cases are presented in Reference 9.

4.5   Kalman Filter for Observing the System States

4.5.1   Gain Calculation

This section presents a modified Kalman filter to estimate the system states used in the perturbation feedback scheme of Section 4.4. The approach presented here involves the use of linearized plant equations similar to those used for the perturbation feedback.
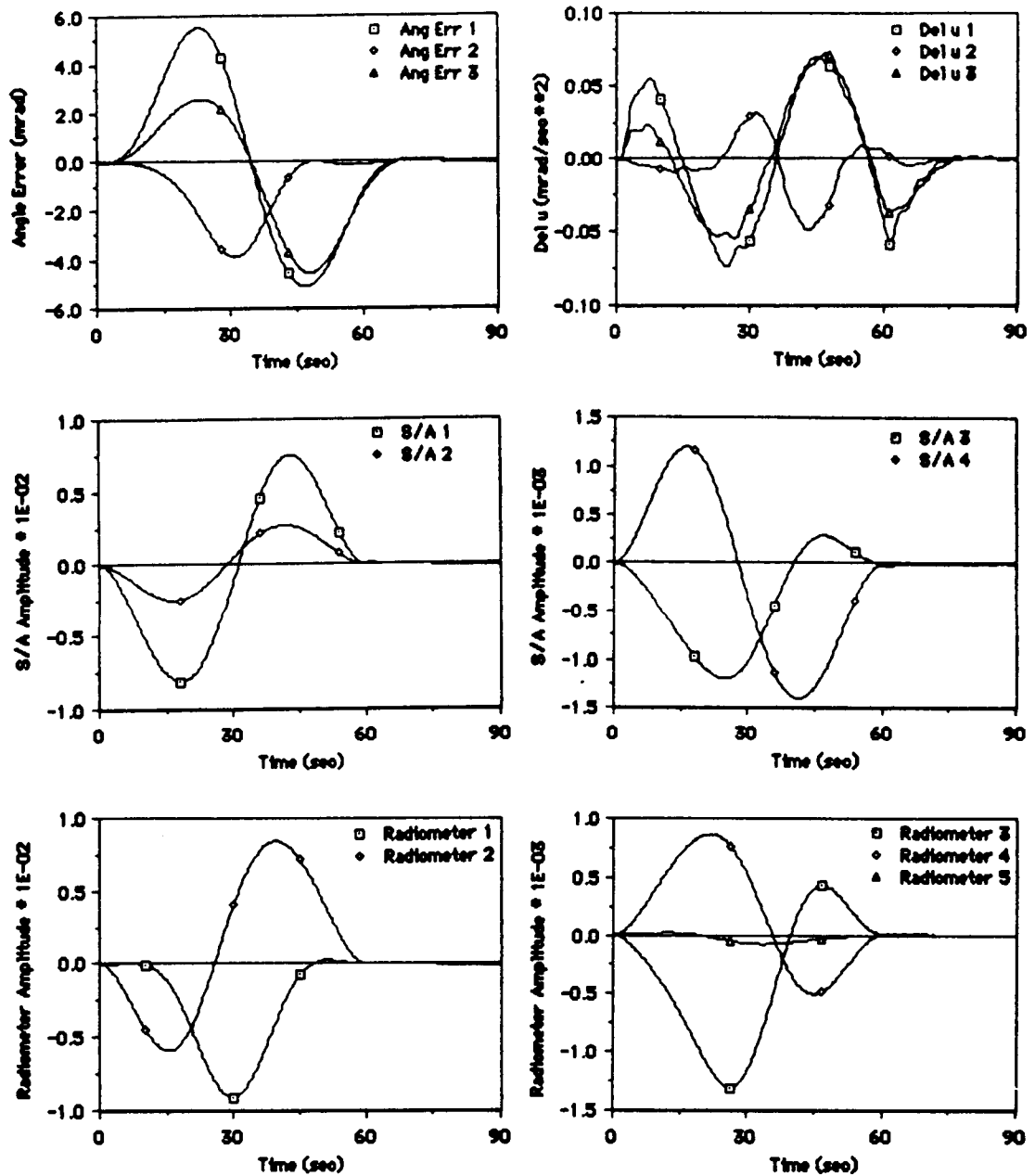
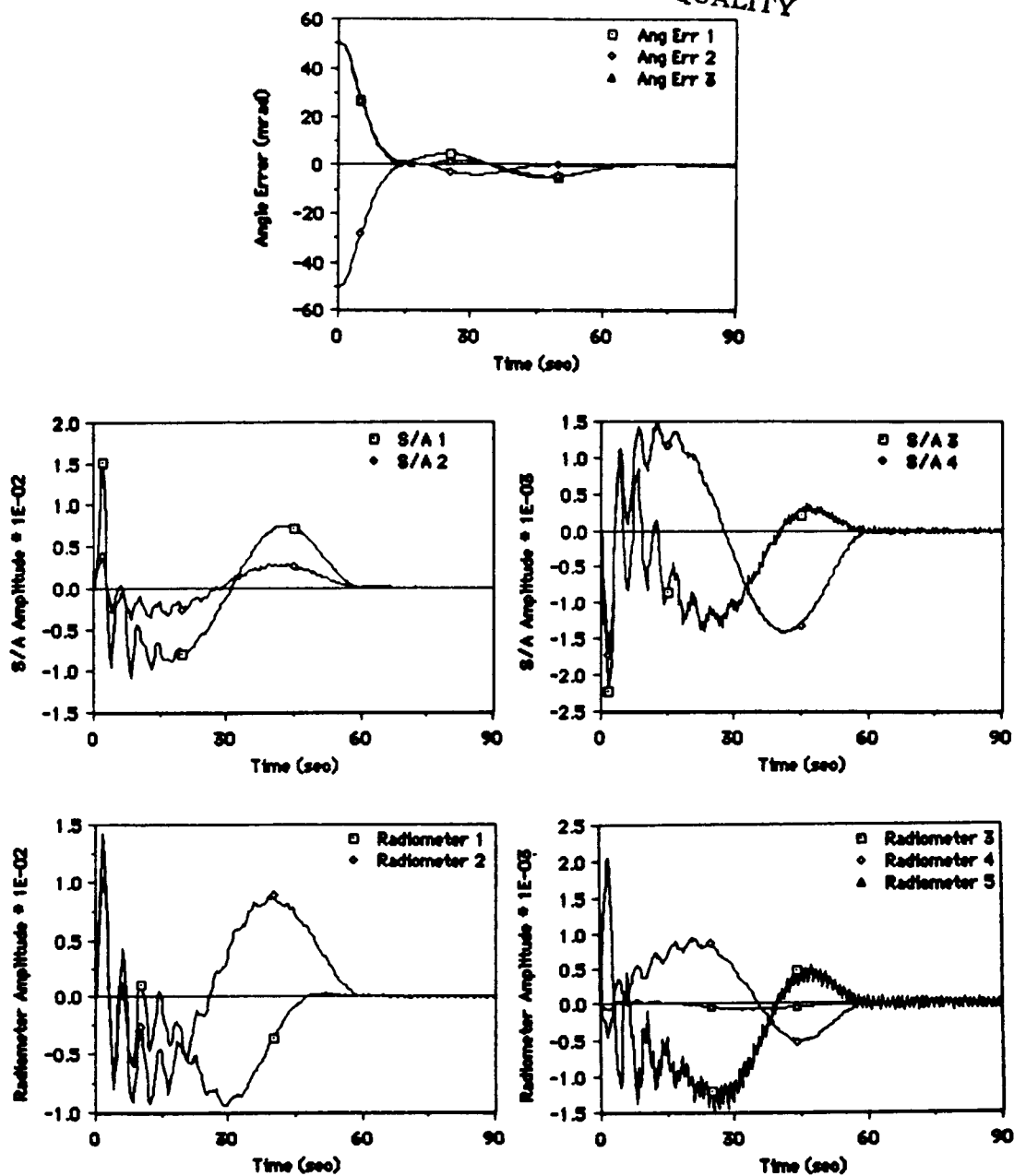Figure 4-6.   Case 1.   'Nominal' Perturbation Feedback

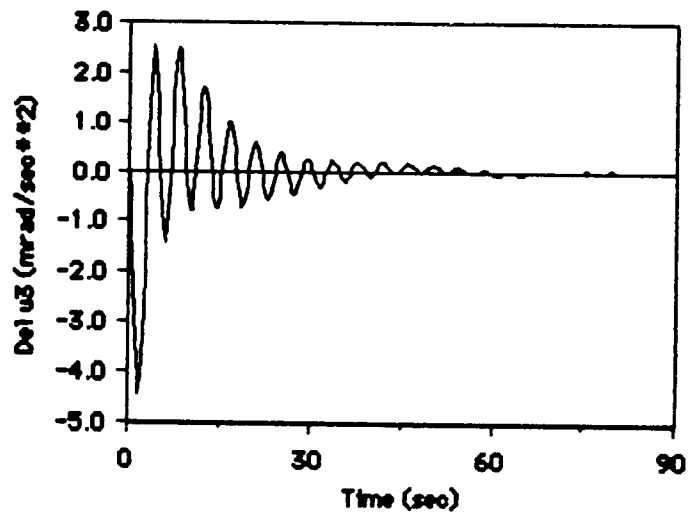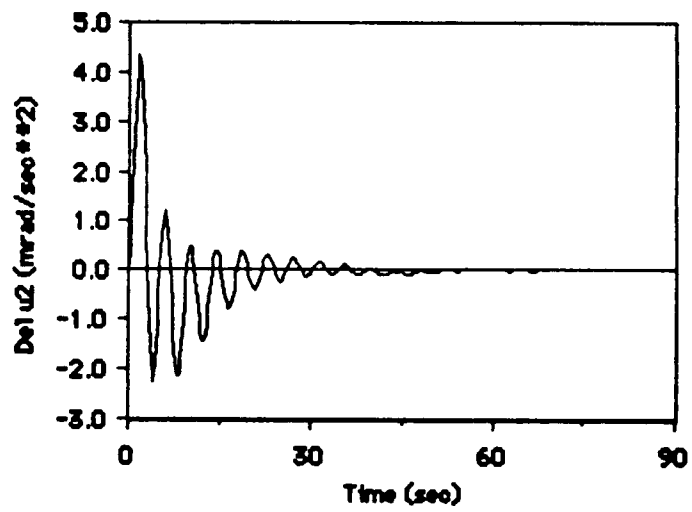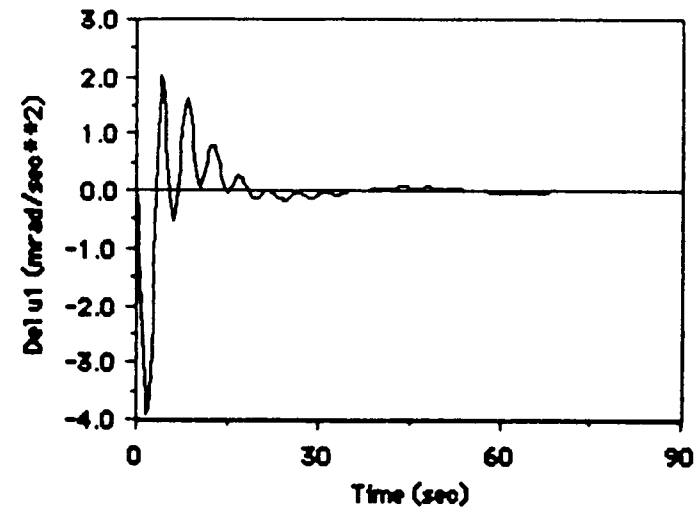Figure 4-7.   Case 2.   Off-Nominal Initial Angles

Figure 4-8.   Pseudo-Control Corrections for Case 2

Let us assume that in addition to the system dynamics matrix, $A^{(i)}$, and the control influence matrix, $B^{(i)}$, of (4.4.2), the measurement influence matrix, $C^{(i)}$, is also linearized about the nominal trajectory at several points in time. For the calculation of the Kalman gains, let us assume that the linearized plant dynamics and measurements are subjected to Gaussian white noise disturbances:

$$\dot{x}(t) = A^{(i)}x(t) + B^{(i)}u_o(t) + w(t) , \qquad t \approx t_i , \qquad (4.5.1)$$

and

$$y(t) = C^{(i)}x(t) + v(t) , \qquad (4.5.2)$$

where

$$E\left[\left\{\begin{matrix} w(t_1) \\ v(t_1) \end{matrix}\right\}\left\{\begin{matrix} w(t_2) \\ v(t_2) \end{matrix}\right\}^T\right] = \begin{bmatrix} \bar{Q} & 0 \\ 0 & \bar{R} \end{bmatrix}\delta(t_2-t_1) ,$$

$$E[w(t)] = 0 , \quad \text{and } E[v(t)] = 0 .$$

Let us assume a linear estimator of the form

$$\dot{\hat{x}}(t) = A^{(i)}\hat{x}(t) + B^{(i)}u_o(t) + K^{(i)}[y(t) - C^{(i)}\hat{x}(t)] , \qquad (4.5.3)$$

where $K^{(i)}$ is a set of constant observer gains.

It can be shown that the gain matrix which minimizes the error covariance is given by

$$K^{(i)} = X_{ss}^{(i)}[C^{(i)}]^T\bar{R}^{-1} , \qquad (4.5.4)$$

where $X_{ss}^{(i)}$ is the steady-state error covariance matrix for the linearized plant:

$$0 = AX_{ss} + X_{ss}A^T - X_{ss}C^T\bar{R}^{-1}CX_{ss} + \bar{Q} , \qquad (4.5.5)$$

and the superscript notation has been dropped.

During the simulation of the estimator, the variables $A^{(i)}$, $B^{(i)}$, $C^{(i)}$, and $K^{(i)}$ are linearly interpolated as in Section 4.4 for the perturbation feedback gains.

4.5.2 Numerical Results

As in Section 4.4.2, the flexible plant is linearized about the rigid body nominal solution at 12 second intervals for the results of this section. The measurement variables used for the results of this section are the spacecraft Euler angles relative to the inertial frame; the body angular velocities of the spacecraft bus; the out-of-plane deformations and velocities of diagonally opposite corners of the solar array (points 3 and 6); and the deformations and velocities of two points on the radiometer (points 9 and 10). It is assumed that raw data from sensors, such as accelerometers on the solar array, has already been processed to provide the measurements stated above. Due to the limited scope of this study, the sensor locations are not optimized for best performance. The process and measurement noise variances are chosen as small percentages of the peak values experienced in the 'nominal' Case 1 of Section 4.4.2. Case 3 (Figs. 4-9 through 4-11) shows the result of replacing the true state variable by the state estimate in computing the perturbation feedback for Case 1 of Section 4.4. Figure 4-9 shows that the Euler angles converge to their desired final values of 1 radian, with slight overshoot for the first and third Euler angles. The sensor point deformations shown in Figure 4-9 have very smooth profiles which converge to zero near the final maneuver time. Points 3 and 6 correspond to the two corners of the solar array, and points 9 and 10 correspond to two points near the center of the radiometer. The pseudo-control corrections of Figure 4-10 have higher peak values than the corresponding plots in Case 1 of Section 4.4. The angular estimate errors show the result of linearization at discrete points in time. One remedy is to linearize the plant at shorter time intervals. A better solution is to perform
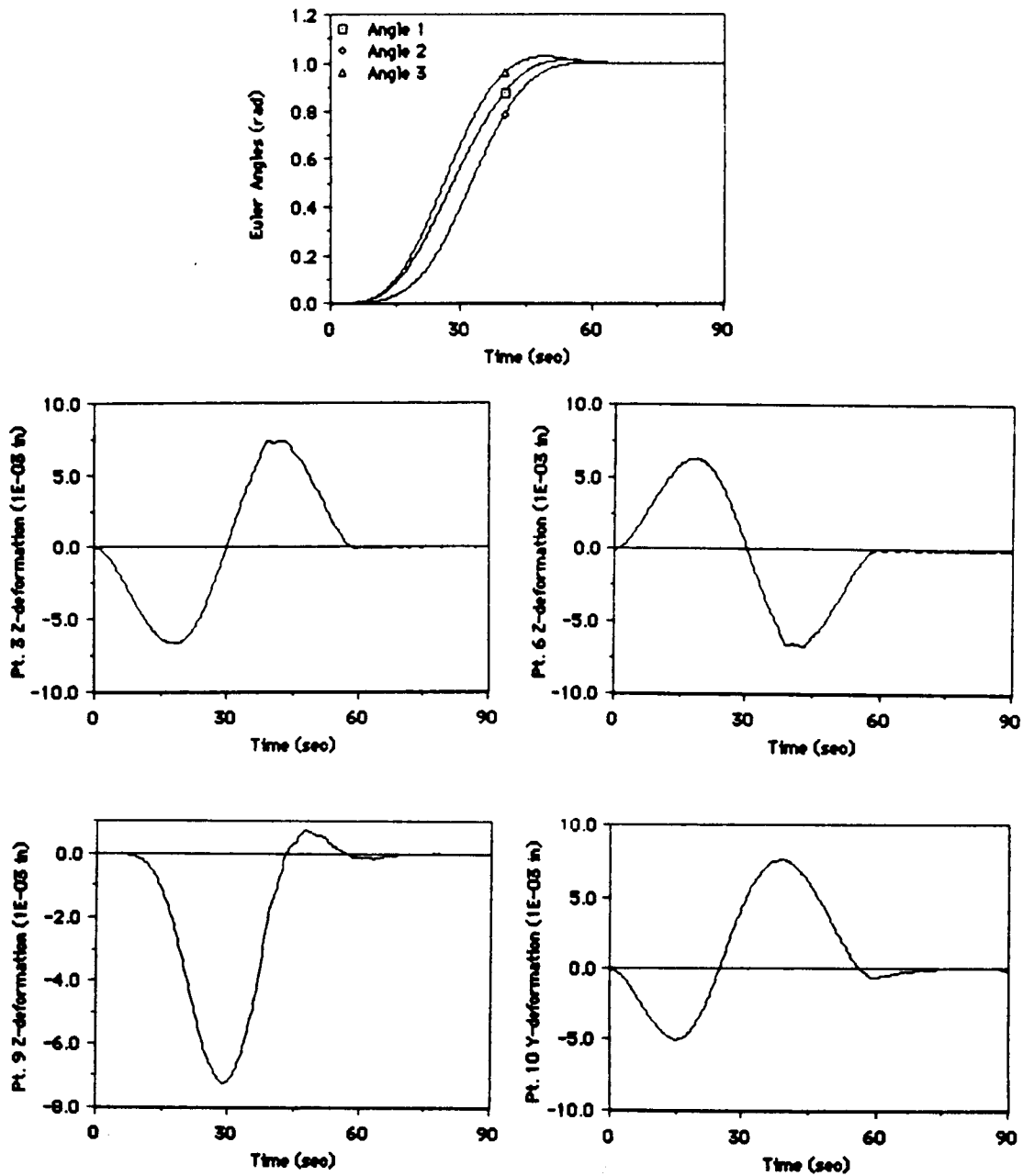
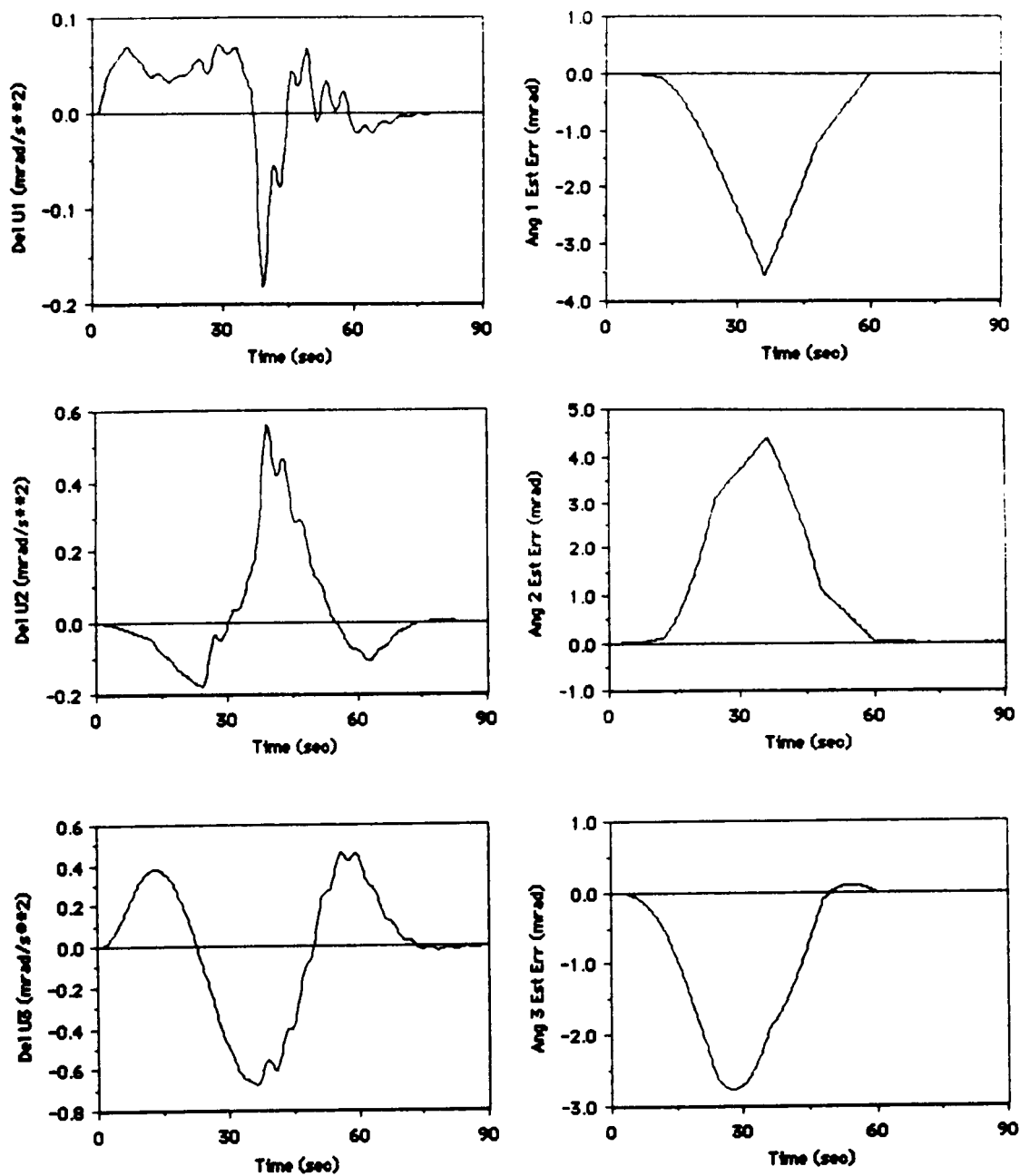Figure 4-9.   Euler Angles and Sensor Point Deformations
For Case 3

Figure 4-10.   Pseudo-Control Corrections and Angle
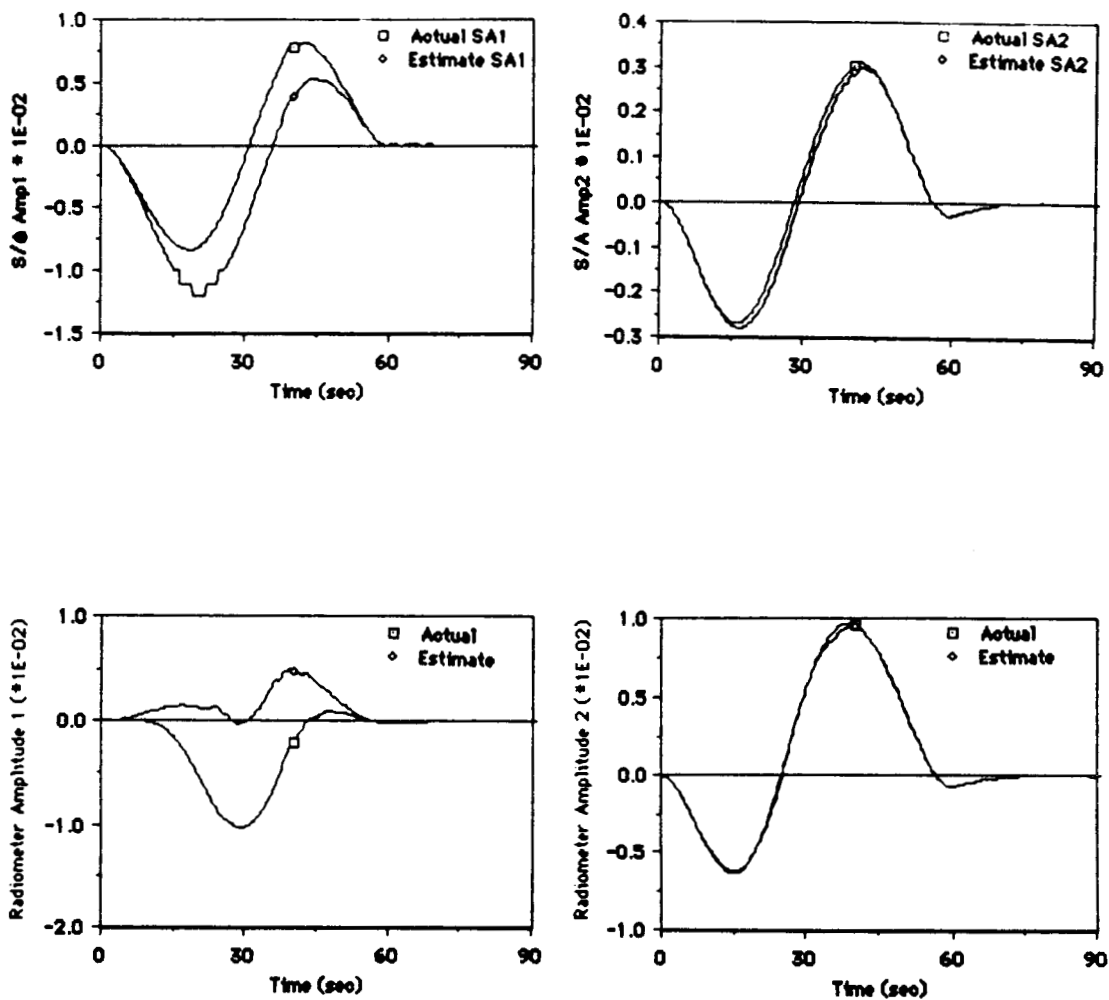Estimate Errors for Case 3

Figure 4-11. Solar Array and Radiometer Modal Amplitudes
and Their Estimates for Case 3

perturbation estimation about the nominal rigid body trajectory rather than estimation for the entire state. Figure 4-11 shows the amplitudes of the controlled modes and their estimates. One can see that the first solar array and radiometer modes are not estimated very well. This is due to observation spillover from the residual modes. In order to minimize the effects of observation spillover, one must choose optimal locations for the sensor points. Since there are 271 grid points on the radiometer with 5 modes, and 1000 grid points on the solar array with 4 modes (the original model has 15 modes), and six degrees of freedom to choose from, an automated procedure must be used for the selection of sensor locations [4,37]. However, this is beyond the scope of the current study. Additional examples are shown in Reference 9.

SECTION 5

SUMMARY AND CONCLUSIONS

This report has covered three different, yet interrelated topics. Section 2 has dealt with a new class of closed-form solutions for finite-time linear-quadratic optimal control problems. These closed-form solutions are used in Section 3, which presents the solution for the neighboring extremal path problem, as applied to spacecraft slewing maneuvers. Section 4 has dealt with general nonlinear slewing maneuvers for flexible spacecraft, for which the results of Section 3 are useful when the terminal conditions are slightly perturbed. A more detailed summary of each section follows.

Section 2 has dealt with a new class of closed-form solutions for finite-time linear-quadratic optimal control problems where the plant is linear time-invariant. This class of closed-form solutions is based on Potter's solution, which consists of a steady-state plus transient term, for the differential matrix Riccati equation. Five basic differential equations are identified for the solution of finite-time linear-quadratic optimal control problems. Closed-form solutions are presented for these five basic differential equations, and example control problems are presented where these solutions are used to obtain closed-form analytic expressions for the feedback gains, state trajectories, control trajectories, and residual state trajectories, with the assumptions of perfect plant knowledge, and perfect state estimation.

For each example control problem, comparisons are made with closed-form solutions based on the Kalman-Englar method, and on the state transition matrix. For each case, it is found that the new class of closed-form solutions is more efficient than the Kalman-Englar type of solution based on the state transition matrix. Furthermore, it is well known that the Kalman-Englar solution for the Riccati matrix is numerically unstable when the propagation time-step is large, or when the

Riccati solution is not symmetrized at each time-step. Such numerical problems do not occur in Potter's solution for the Riccati matrix. Thus, it seems that the new class of solutions is numerically superior to the Kalman-Englar type of solutions for feedback gains and state transition matrix solutions for state and control trajectories. However, a rigorous analysis of the numerical stability and error propagation characteristics of the new class of closed-form solutions remains a topic for further research.

The relationship between the new class of solutions and the state transition matrix solutions is illustrated by means of reducing subspace transformations for the Hamiltonian matrix.

The closed-form solutions developed in Section 2 are applied to the free-final-time neighboring extremal path problem with linear terminal constraints, a quadratic performance index, and a linear time-invariant plant. Closed-form solutions are presented for the perturbation feedback gains which cause the system to follow a neighboring extremal path when subjected to small perturbations in the initial conditions and terminal constraints. Numerical experiments indicate that slight numerical modifications can greatly reduce the sensitivity of the feedback gains near the final time. An extension is shown for using the closed-form solutions for problems with nonlinear plants.

Section 4 has presented a formulation for general nonlinear slewing maneuvers for flexible spacecraft, whereby a rigid body nominal control profile is applied while a perturbation feedback controller limits the flexible body response and controls the plant to follow the rigid body nominal trajectory. The use of control smoothing in both the rigid body nominal solution and the perturbation feedback controller greatly reduces the excitation to the elastic degrees of freedom.

Numerical results show that the break frequency used for the control smoothing formulation for the rigid body nominal solution should be linked to the maneuver time in order to produce good results. Numerical results for the perturbation feedback controller show that it

performs very well under off-nominal conditions for a 60 second maneuver. For further research, it is recommended that the maneuver time be shortened so that the break frequency for the rigid body nominal solution overlaps some of the structural frequencies. Such a case should prove challenging, since this would involve more interaction between the rigid modes and the elastic modes.

A modified Kalman filter is presented for estimating the system states. Numerical results indicate that the approach is feasible. However, for further work, it is recommended that a sensor location optimization be performed to minimize the possibliity of observation spillover. Furthermore, a perturbation estimation approach may be used, whereby one estimates the state perturbations rather than the states themselves.

For maneuvers where the desired final conditions are different from the nominal final conditions, one must use the optimal perturbation feedback of Section 3, with the modifications for nonlinear plants. Such an approach would result in near-optimal time-varying feedback gains, using the same type of linearized plant as used for the results of Section 4.

LIST OF REFERENCES

[1] Athans, M. and Falb, P.L., Optimal Control, McGraw-Hill, New York, 1966.

[2] Bartels, R.H. and Stewart, G.W., "A Solution of the Equation AX + XB = C," Communications of ACM, Vol. 15, No. 9, September 1972, pp. 820-826.

[3] Bauer, T.P., Wood, L.J., and Caughey, T.K., "Gain Indexing Schemes for Low-Thrust Perturbation Guidance," Journal of Guidance, Control, and Dynamics, Vol. 6, No. 6, November-December 1983, pp. 518-525.

[4] Bodley, C.S., Devers, A.D., Park A.C., and Frisch, H.P., "A Digital Computer Program for the Dynamic Interaction Simulation of Controls and Structure (DISCOS)," NASA Technical Paper 1219, Vol. 1, 1978.

[5] Brockett, R.W., Finite Dimensional Linear Systems, John Wiley and Sons, Inc., New York, New York, 1970.

[6] Brown, M.E., "Rapid Slewing Maneuvers of a Flexible Spacecraft Using On/Off Thrusters," Master of Science Thesis, Massachusetts Institute of Technology, September 1983.

[7] Bryson, A.E., Jr. and Ho, Y.C., Applied Optimal Control, Hemisphere Publishing Corp., Washington, D.C., 1975.

[8] Chun, H.M., "Optimal Distributed Control of a Flexible Spacecraft During a Large-Angle Maneuver," Master of Science Thesis, Massachusetts Institute of Technology, Cambridge, Massachusetts, 1982.

[9] Chun, H.M., "Large-Angle Slewing Maneuvers for Flexible Spacecraft," PhD dissertation, Massachusetts Institute of Technology, Cambridge, Massachusetts, 1986.

[10] Chun, H.M. and Turner, J.D., "A Simple Algorithm for the Selection of Terminal Penalty Weight Matrices," Journal of Guidance, Control, and Dynamics, Vol. 9, No. 4, July-August 1986, pp. 503-505.

[11] Davison, E.J., "The Numerical Solution of $\dot{X} = A_1 X + X A_2 + D$, $X(0) = C$," IEEE Transactions on Automatic Control, Vol. AC-20, No. 4, August 1975, pp. 566-567.

[12] Frisch, H.P., "A Vector-Dyadic Development of the Equations of Motion for N-Coupled Flexible Bodies and Point Masses," NASA TN D-8047, August 1975.

[13] Golub, G.H., Nash, S., and Van Loan, C.F., "A Hessenburg-Schur Method for the Problem AX + XB = C," _IEEE Transactions on Automatic Control_, Vol. AC-24, No. 6, December 1979, pp. 909-913.

[14] Hegg, D.R., et al, "ACOSS Eleven-Fourth Semiannual Technical Report," Vol. 2, CSDL-R-1648, Contract No. F30602-81-C-0180, The Charles Stark Draper Laboratory, Inc., Section 2, August 1983.

[15] Ho, J.Y.L., "Direct Path Method for Flexible Multibody Spacecraft Dynamics," _Journal of Spacecraft and Rockets_, Vol. 14, February 1977, pp. 102-110.

[16] Ho, J.Y.L., and Herber, D.R., "Development of Dynamics and Control Simulation of Large Flexible Space Systems," _Journal of Guidance, Control, and Dynamics_, Vol. 8, No. 3, May-June 1985, pp. 374-383.

[17] Jamshidi, A.H., "An Overview of the Solutions of the Algebraic Matrix Riccati Equation and Related Problems," _Large Scale Systems: Theory and Application_, North-Holland Publishing Co., Vol. 1, No. 3, August 1980, Singh M.G. and Sage, A.P. (editors), pp. 167-192.

[18] Kalman, R.E., and Englar, T.S., "A User's Manual for the Automatic Synthesis Program (Program C)," NASA CR-475, 1966.

[19] Kane, T.R., Ryan, R.R., and Banerjee, A.K., "Dynamics of a Beam Attached to a Moving Base," Paper AAS 85-390, _AAS/AIAA Astrodynamics Specialist Conference_, Vail, Colorado, August 12-15, 1985.

[20] Kelley, H.J., "An Optimal Guidance Approximation Theory," _IEEE Transactions on Automatic Control_, Vol. AC-9, October 1964, pp. 375-380.

[21] Kwakernaak, H., and Sivan, R., _Linear Optimal Control Systems_, John Wiley and Sons, Inc., New York, New York, 1972.

[22] Martensson, K., "On the Matrix Riccati Equation," _Information Sciences_, Vol. 3, 1971, pp. 17-49.

[23] Osborne, M.R., "On Shooting Methods for Boundary Value Problems," _Journal of Mathematical Analysis and Applications_, Vol. 27, 1969, pp. 417-433.

[24] Pace, I.S., and Barnett, S., "Comparison of Numerical Methods for Solving Lyapunov Matrix Equations," _International Journal of Control_, Vol. 15, No. 5, 1972, pp. 907-915.

[25] Potter, J.E., "Matrix Quadratic Solutions," _SIAM Journal of Applied Mathematics_, Vol. 14, No. 3, 1964, pp. 496-501.

[26] Potter, J.E., "A Matrix Equation Arising in Statistical Filter Theory," NASA CR-270, 1965.

[27]   Potter, J.E., and Vander Velde, W.E., "Optimal Mixing of Gyroscope and Star Tracker Data," *Journal of Spacecraft and Rockets*, Vol. 5, May 1968, pp. 536-540.

[28]   Prussing, J.E., "A Simplified Method for Solving the Matrix Riccati Equation," *International Journal of Control*, Vol. 15, No. 5, 1972, pp. 995-1000.

[29]   Richter, S.L., and DeCarlo, R.A., "Continuation Methods: Theory and Applications," *IEEE Transactions on Circuits and Systems*, Vol. CAS-30, No. 6, June 1983, pp. 347-352.

[30]   Roberts, S.M., and Shipman, J.S., *Two-Point Boundary Value Problems: Shooting Methods*, American Elsevier Publishing Company, New York, New York, 1972.

[31]   Serbin, S.M., and Serbin, C.A., "A Time-Stepping Procedure for $\dot{X} = A_1 X + X A_2 + D$, $X(0) = C$," *IEEE Transactions on Automatic Control*, Vol AC-25, No. 6, December 1980, pp. 1138-1141.

[32]   Singh, VanderVoort, R.J., and Likins, P.W., "Dynamics of Flexible Bodies in Tree Topology -- A Computer Oriented Approach," Paper No. AIAA-84-1024, *AIAA/ASME/ASCE 25th Structures, Structural Dynamics and Materials Conference*, Palm Springs, California, May 14-18, 1984.

[33]   Speyer, J.L., and Bryson, A.E., Jr., "A Neighboring Optimum Feedback Control Scheme Based on Estimated Time-to-Go with Application to Re-Entry Flight Paths," *AIAA Journal*, Vol. 6, No. 5, May 1968, pp. 769-776.

[34]   Turner, J.D., "Optimal Large Angle Maneuvers for Large Flexible Space Structures," Ph.D. Dissertation, VPI&SU, Blacksburg, Virginia, 1980.

[35]   Turner, J.D., Messac, A., and Junkins, J.L., "Finite Time Matrix Convolution Integral Sensitivity Calculations," *Journal of Guidance, Control, and Dynamics*, Vol. 11, No. 2, March-April 1988.

[36]   Vadali, S.R., Kraige, L.G., and Junkins, J.L., "New Results on the Optimal Spacecraft Attitude Maneuver Problem," *Journal of Guidance, Control, and Dynamics*, Vol. 7, No. 3, May-June 1984, pp. 378-380.

[37]   Vander Velde, W.E., and Carignan, C.R., "Number and Placement of Control System Components Considering Possible Failures," *Journal of Guidance, Control, and Dynamics*, Vol. 7, No. 6, November-December 1984, pp. 703-709.

[38]   Vaughan, D.R., "A Negative Exponential Solution for the Matrix Riccati Equation," *IEEE Transactions on Automatic Control*, Vol. AC-14, No. 1, 1969, pp 72-75.

Standard Bibliographic Page

1. Report No. NASA CR-4123	2. Government Accession No.	3. Recipient's Catalog No.
4. Title and Subtitle Large-Angle Slewing Maneuvers for Flexible Spacecraft		5. Report Date February 1988
		6. Performing Organization Code
7. Author(s) Hon M. Chun and James D. Turner		8. Performing Organization Report No. CR-R-016
9. Performing Organization Name and Address Cambridge Research, A Division of Photon Research Associates, Inc. 1033 Massachusetts Avenue Cambridge, Massachusetts 02138		10. Work Unit No. 585-01-21-01
		11. Contract or Grant No. NAS1-18098
12. Sponsoring Agency Name and Address National Aeronautics and Space Administration Langley Research Center Hampton, Virginia 23665-5225		13. Type of Report and Period Covered Contractor Report
		14. Sponsoring Agency Code

15. Supplementary Notes
Langley Technical Monitor: Jer-Nan Juang Final Report

16. Abstract

This report presents a new class of closed-form solutions for finite-time linear-quadratic optimal control problems. This class of closed-form solutions involves Potter's solution for the differential matrix Riccati equation, which assumes the form of a steady-state plus transient term. Illustrative examples are presented which show that the new solutions are more computationally efficient than alternative solutions based on the state transition matrix. As an application of the closed-form solutions, the neighboring extremal path problem is presented for a spacecraft retargeting maneuver where a perturbed plant with off-nominal boundary conditions now follows a neighboring optimal trajectory. The perturbation feedback approach is further applied to three-dimensional slewing maneuvers of large flexible spacecraft. For this problem, the nominal solution is the optimal three-dimensional rigid body slew. The perturbation feedback then limits the deviations from this nominal solution due to the flexible body effects. The use of frequency-shaping in both the nominal and perturbation feedback formulations reduces the excitation of high-frequency unmodeled modes. A modified Kalman filter is presented for estimating the plant states.

17. Key Words (Suggested by Authors(s)) Closed-Form Solutions, Continuation Method, Large Space Structures, Multibody Dynamics, Optimal Control Problems, Perturbation Feedback, Frequency Shaping, Three-Dimensional Slews	18. Distribution Statement Unclassified – Unlimited Subject Category 39		
19. Security Classif.(of this report) Unclassified	20. Security Classif.(of this page) Unclassified	21. No. of Pages 86	22. Price A05